Cell Reports
Medicine

Article

Balance between immunoregulatory B cells and plasma cells drives pancreatic tumor immunity

Graphical abstract

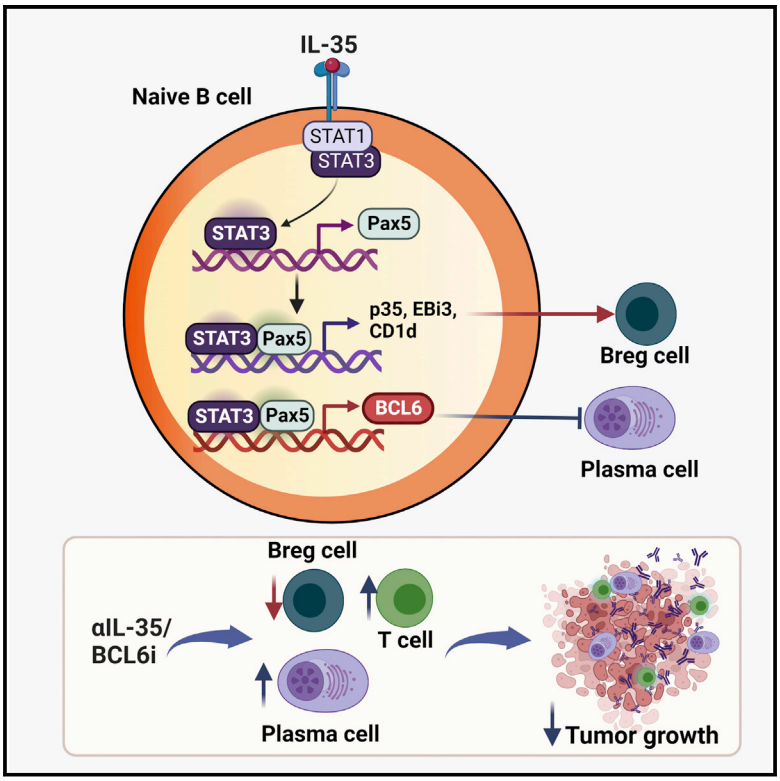

Highlights

- Balance between regulatory B cells and plasma cells shapes pancreatic tumor growth
- Cancer primes naive B cells toward regulatory B cell differentiation
- IL-35 drives B cell reprogramming via formation of a pSTAT3-Pax5 complex
- IL-35/BCL6 blockade in naive B cells enhances αPD1 efficacy

Authors

Bhalchandra Mirlekar, Yan Wang, Sirui Li, ..., William Y. Kim, Jen Jen Yeh, Yuliya Pylayeva-Gupta

Correspondence

yuliyap1@email.unc.edu

In brief

Mirlekar et al. report that IL-35-driven transcriptional reprogramming of naive B cells in pancreatic cancer shifts B cell development away from effector plasma cell responses toward an immunoregulatory phenotype. Inhibition of IL-35 or BCL6 in naive B cells limits tumor growth by potentiating anti-tumor plasma and T cell responses.

Mirlekar et al., 2022, Cell Reports Medicine *3*, 100744
September 20, 2022
https://doi.org/10.1016/j.xcrm.2022.100744

CellPress

Cell Reports Medicine

CellPress
OPEN ACCESS

Article

Balance between immunoregulatory B cells and plasma cells drives pancreatic tumor immunity

Bhalchandra Mirlekar,[1] Yan Wang,[1] Sirui Li,[1] Mi Zhou,[1] Sarah Entwistle,[1] Tristan De Buysscher,[2] Ashley Morrison,[1] Gabriela Herrera,[1] Cameron Harris,[1] Benjamin G. Vincent,[1,3] Jenny P.- Y. Ting,[1,3,4] Naim Rashid,[1,5] William Y. Kim,[1,6] Jen Jen Yeh,[1,7] and Yuliya Pylayeva-Gupta[1,4,8,*]

[1]Lineberger Comprehensive Cancer Center, The University of North Carolina at Chapel Hill School of Medicine, Chapel Hill, NC, USA
[2]Bioinformatics and Analytics Research Collaborative, The University of North Carolina at Chapel Hill School of Medicine, Chapel Hill, NC, USA
[3]Department of Microbiology and Immunology, The University of North Carolina at Chapel Hill School of Medicine, Chapel Hill, NC, USA
[4]Department of Genetics, The University of North Carolina at Chapel Hill School of Medicine, Chapel Hill, NC, USA
[5]Department of Biostatistics, The University of North Carolina at Chapel Hill School of Medicine, Chapel Hill, NC, USA
[6]Department of Medicine-Oncology, The University of North Carolina at Chapel Hill School of Medicine, Chapel Hill, NC, USA
[7]Department of Surgery, The University of North Carolina at Chapel Hill School of Medicine, Chapel Hill, NC, USA
[8]Lead contact
*Correspondence: yuliyap1@email.unc.edu
https://doi.org/10.1016/j.xcrm.2022.100744

SUMMARY

Plasma cell responses are associated with anti-tumor immunity and favorable response to immunotherapy. B cells can amplify anti-tumor immune responses through antibody production; yet B cells in patients and tumor-bearing mice often fail to support this effector function. We identify dysregulated transcriptional program in B cells that disrupts differentiation of naive B cells into anti-tumor plasma cells. The signaling network contributing to this dysfunction is driven by interleukin (IL) 35 stimulation of a STAT3-PAX5 complex that upregulates the transcriptional regulator BCL6 in naive B cells. Transient inhibition of BCL6 in tumor-educated naive B cells is sufficient to reverse the dysfunction in B cell differentiation, stimulating the intra-tumoral accumulation of plasma cells and effector T cells and rendering pancreatic tumors sensitive to anti-programmed cell death protein 1 (PD-1) blockade. Our findings argue that B cell effector dysfunction in cancer can be due to an active systemic suppression program that can be targeted to synergize with T cell-directed immunotherapy.

INTRODUCTION

Harnessing the power of the immune system to fight cancer has proved both inspirational and challenging. Significant effort has been centered on T cells as the predominant cancer-killing immune cell type.[1,2] However, accumulating data point to a critical role for B cell-mediated anti-tumor immunity in the response to immunotherapy.[3–6] These recent studies in patients and mouse models revealed that tertiary lymphoid structure (TLS) formation and plasma cell expansion can be a strong predictor of patient survival and immunotherapy efficacy. Nevertheless, such responses are heterogeneous and the mechanisms that restrict B cell-directed anti-tumor function in cancer remain poorly understood.[7] This heterogeneity in B cell responses is also evident in pancreatic ductal adenocarcinoma (PDAC), an aggressive and deadly disease, characterized by rampant immunosuppression and resistance to immunotherapy, as simple evaluation of B cell infiltration could not distinguish between positive, neutral, or negative patient prognoses.[8–13]

B cells frequently infiltrate human tumors, and the intra-tumoral abundance of plasma cells can correlate with improved patient prognosis. However, some tumors are devoid of plasma B cells, and strategies to enhance anti-tumor B cell responses are needed.[14] Tumor-promoting B cells are typically defined by their ability to modulate immune tolerance via production of immunosuppressive cytokines and/or direct interaction with T cells.[15–20] On the other hand, in both oncologic and autoimmune diseases, immunoregulatory B cells (Bregs) can be found as diverse interleukin (IL)-10$^+$, IL-35$^+$ and/or transforming growth factor (TGF) β^+ B cell populations.[15,17,21–28] There is a significant knowledge gap in our understanding of how effective anti-tumor B cell responses versus regulatory responses are generated. The transcriptional and signaling mechanisms that regulate B cell differentiation in malignancy are not well understood but have implications for the development of B cell-targeted immunotherapies.

Here, we set out to examine the development of immunosuppressive and effector B cell responses in the context of PDAC. Using human patient data, genetically engineered models, B cell profiling, and functional assays, we demonstrate that IL-35$^+$ B cells can inversely correlate with plasma cell frequency in PDAC. Using transcriptional profiling of naive B cells, we show that IL-35 production by B cells in cancer controls a distinct transcriptional state of naive B cells that antagonizes plasma cell differentiation through

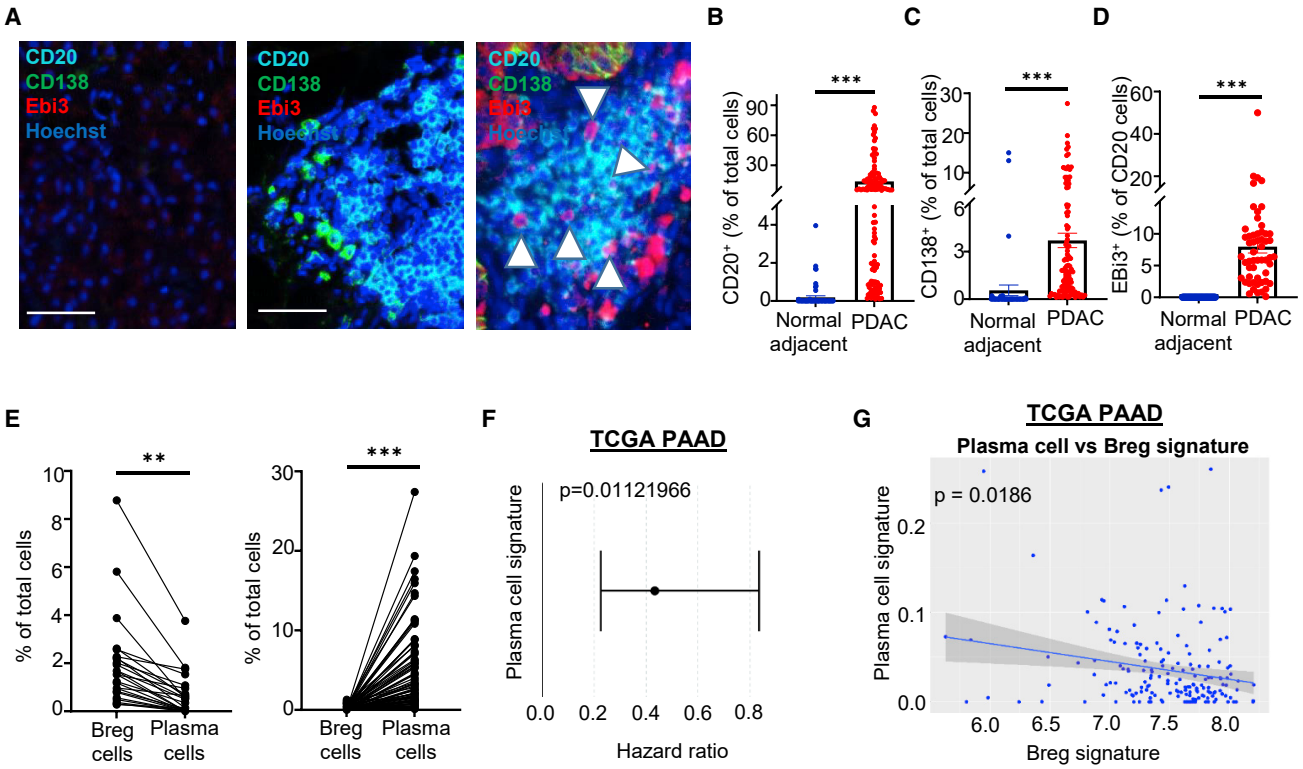

Figure 1. Increased accumulation of B cell subsets in human PDAC

(A) Representative immunofluorescence staining for CD20, CD138, and Ebi3 in samples of normal adjacent (left) and human PDAC. $CD20^+Ebi3^+$ B cells are indicated by arrowheads. Scale bars, 50 μm.

(B) Quantification of the frequency of $CD20^+$ cells in human PDAC (N = 56) and adjacent normal tissues (N = 23).

(C) Quantification of the frequency of $CD138^+$ cells in human PDAC and adjacent normal tissues.

(D) Quantification of the frequency of $CD20^+Ebi3^+$ cells in human PDAC and adjacent normal tissues.

(E) Paired analysis of intra-tumoral $CD20^+Ebi3^+$ Bregs and $CD138^+$ plasma cells.

(F) Association with survival via Cox proportional hazards (PH) regression analysis of plasma cell signature in TCGA PAAD dataset.

(G) Correlation of cancer Breg signature with plasma cell signature in PAAD (TCGA). For immunofluorescence quantification, three fields per sample were counted. Error bars indicate SEM, p values were calculated using Student's t test (unpaired, two tailed); NS, not significant; $^{**}p < 0.01$; $^{***}p < 0.001$.

stabilized expression of the B cell lineage-defining transcription factors Pax5 and Bcl6. Targeting Bcl6 in naive B cells subsequently leads to increased intra-tumoral plasma cells and overcomes resistance to immunotherapy, leading to tumor growth control. We thereby show that transcriptional reprogramming of naive B cells can serve as a targetable node that regulates the balance between effector and Breg lineage function and tumor immunity in PDAC.

RESULTS

Plasma and Breg subset distribution in human PDAC

To characterize the relationship between B cell subtypes in PDAC patients, we assessed the distribution of plasma and Bregs. To quantify abundance, we used multiplex immunofluorescence to analyze primary human PDAC tissue samples for the presence of $CD20^+$ B cells, CK^-CD138^+ plasma cells, and $CD20^+Ebi3^+$ Breg (Figures 1A and S1). Compared with normal adjacent tissues, PDAC samples had increased numbers of total B cells, as well as increases in overall plasma and Breg abundance (Figures 1B–1D). Analysis of relative frequencies of plasma and Breg cells in each sample revealed a significant negative correlation (Figure 1E). Frequency of plasma cells has previously been linked to improved survival prognosis in melanoma and ovarian cancers.[29–32] To better understand how plasma cell frequency related to survival in patients with pancreatic cancer, we evaluated reported plasma and Breg signatures in patients with PDAC (PAAD) from The Cancer Genome Atlas (TCGA) and found that plasma cell signature correlated with better survival (Figure 1F).[28,33] Consistent with immunofluorescence-based quantification, we observed a significant negative correlation between regulatory and plasma cell signatures in PAAD (Figure 1G) as well as patients in lung adenocarcinoma (LUAD) and colorectal adenocarcinoma (COAD) (Figure S2) cohorts. Collectively, these data demonstrate a positive correlation between plasma cell abundance and prognosis in PDAC and reveal a negative relationship between regulatory and plasma cell abundance in several major cancer types. These observations raised the possibility that B cell differentiation programs may be altered in cancer.

CellPress
OPEN ACCESS

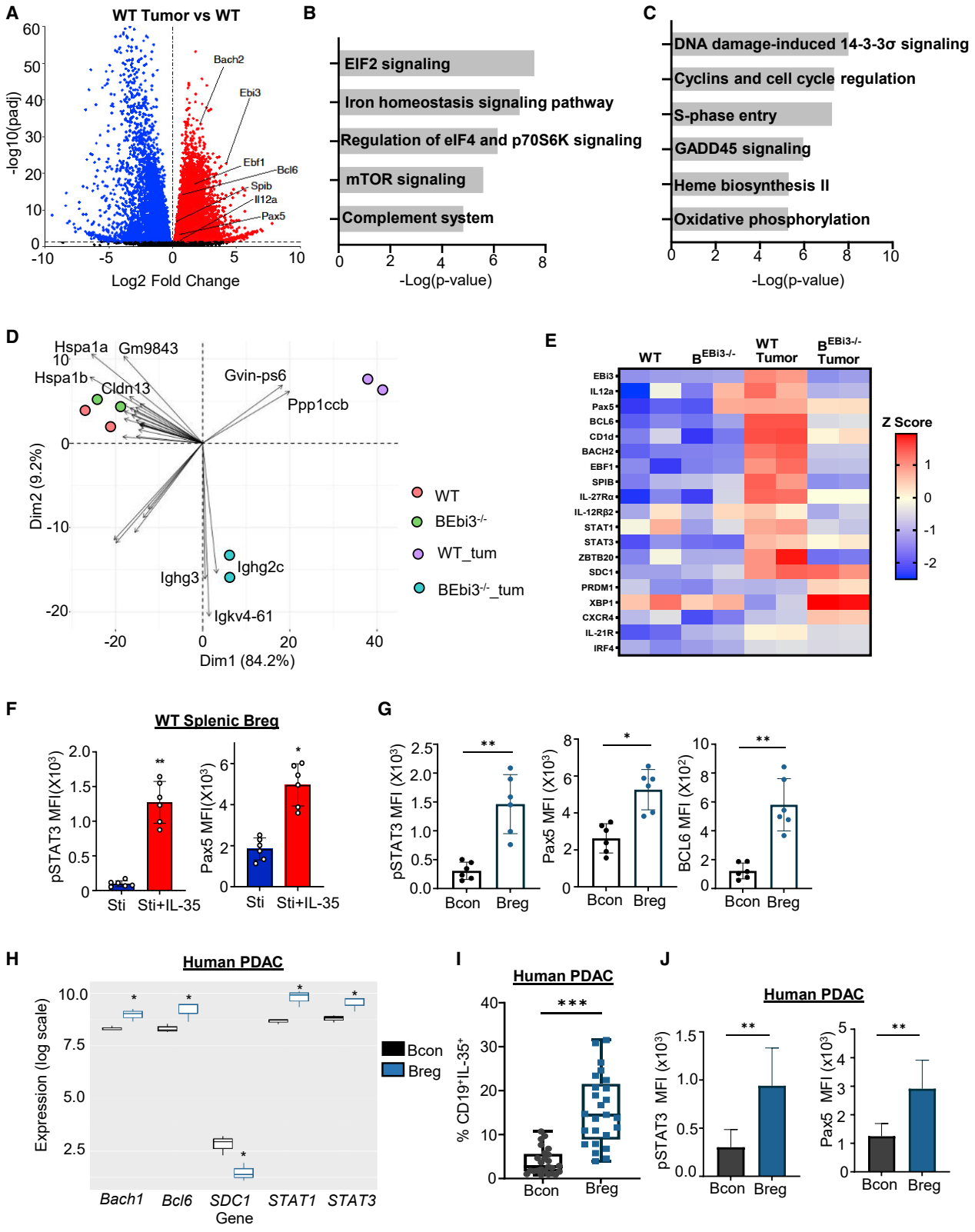

(legend on next page)

Changes in transcriptional profile of tumor-educated naive B cells

To characterize molecular changes to naive B cells in cancer, we conducted RNA sequencing (RNA-seq) of primary naive B cells from control or orthotopic tumor-bearing mice (tumor cells contain mutations in *Kras*$^{G12D/+}$;*TP53*$^{R172H/+}$;*p48*$^{Cre/+}$ [orthotopic *KPC* (o*KPC*)]).[34,35] Altogether, 6,131 genes were differentially regulated between wild-type (WT) and tumor-educated naive B cells (Figures 2A and S3A). Functional annotation of genes in tumor-educated naive B cells, compared with healthy control naive B cells, was determined by Gene Ontology (GO) analysis. Naive B cells from tumor-bearing mice were uniquely enriched in gene sets associated with EIF2 signaling (for example, *Rpl9*, *Rpl41*), iron homeostasis signaling (*Hmox1*, *Tf*), EIF4 and p70S6K signaling (*Rps3*, *Rps21*), mammalian target of rapamycin (mTOR) signaling, and complement system (*C6*, *C1qa*) (Figure 2B; Table S1). The overall expression levels of the gene sets were decreased, suggesting downregulation of protein translation in tumor-educated naive B cells. Further analysis of the top regulator networks revealed inhibition of IFNG and MYC function (Table S2). Strikingly, we observed simultaneous upregulation of several transcriptional regulators of B cell maturation, including pioneer factor *Ebf1*, *Bcl6*, *Bach2*, *Pax5*, and *Spib*,[36–38] as well as markers associated with inflammation and immunosuppressive Bregs (CD19^{+}CD21^{hi}CD1d^{hi}CD5^{+} and IL12a/Ebi3 [IL-35]-positive B cells)[28] such as *STAT1*, *STAT3*, *Il12a*, *Ebi3*, and *Cd1d* (Figure 2A). As described in autoimmune diseases and consistent with our initial transcriptional analysis, these data suggest that specification of immunosuppressive function in B cells may begin at the naive B cell stage.[21,39] Concurrent upregulation of markers of maturation and immunosuppression suggested that cancer-associated cues may lead to establishment of B cell dysfunction.

The mechanisms that regulate B cell lineage commitment in malignancy are not known and have implications for the development of B cell-targeted immunotherapies. We have previously demonstrated that IL-35^{+} B cells suppress anti-tumor T cell responses to promote pancreatic tumor growth and restrict efficacy of immunotherapy.[22,28] Here, we observed that IL-35 is transcriptionally elevated as early as the naive B cell stage in mice with PDAC (Figure 2A). To understand if IL-35 may play a cell-autonomous role in subverting B cell development, we analyzed RNA-seq data from naive B cells in healthy or cancer-bearing mice, following B cell-specific conditional deletion of IL-35 subunit Ebi3 ($B^{EBi3-/-}$). Loss of EBi3 in B cells resulted in differential expression of 2,753 genes in tumor-educated naive B cells (Figures S3B and S3C). Tumor-educated $B^{EBi3-/-}$ naive B cells were enriched in gene sets associated with DNA damage-induced 14-3-3σ signaling, cyclins and cell cycle regulation, S-phase entry, GADD45 signaling (*Ccnb1*, *Ccnr1*, *Cdk1*, *Ccna2*, *E2f8*), heme biosynthesis (*Cpox*), and oxidative phosphorylation (*MT-CO1*, *MT-CYB*) (Figure 2C). There was an overall decrease in cellular proliferation capacity (Table S3). The top regulator networks included tumor suppressor *TP53*, which was significantly upregulated, possibly accounting for overall reduction in cell cycle progression (Table S4). Principal-component analysis (PCA) indicated tumor-educated naive B cells as distinct from healthy controls with principal component 1 (PC1) separating populations by disease status (Figure 2D). Healthy controls from either WT or $B^{EBi3-/-}$ strains had similar gene expression profiles, suggesting that expression of Ebi3 does not perturb steady-state naive B cell homeostasis. Healthy naive B cells were also characterized by low levels of HSP70 (*Hspa1a* and *Hspa1b*), a recently identified regulatory component in B cell-driven suppression in autoimmunity.[40] Tumor-educated WT naive B cells were characterized by downregulation of *Ppp1ccb*, a component of protein synthesis regulators.[41] Loss of Ebi3 in tumor-educated B cells shifted the gene expression profile along both PC1 and PC2 axes, although did not fully recapitulate healthy naive B cell profiles (Figure 2D). Loading plot analysis determined a set of genes that were most strongly associated with driving directionality of principal components. Increase in immunoglobulin gene expression (*Ighg3*, *Igh2c*, *Igkv4*) preferentially drove PCA differences in tumor-educated $B^{EBi3-/-}$ naive B cells compared with healthy and tumor-educated WT B cells, suggesting initiation of antibody synthesis (Figure 2D). Indeed, top upregulated molecules included immunoglobulin chains, *Il21r*, and *Il4r* (Table S5). Additional analysis showed that tumor-educated $B^{EBi3-/-}$ naive B cells featured a prominent loss of Breg-associated genes *Il12a*, *Ebi3*, and *Cd1d* (Figure 2E). In contrast, the plasma cell specifying transcription factors *Prdm1* and *Xbp1* were significantly elevated in the setting of IL-35 loss (Figure 2E). Thus, in the cancer setting, naive B cells can acquire features associated with cellular stress, translational repression, immunosuppression, and maturation,

Figure 2. Transcriptional profiling identifies disease-specific naive B cell states

(A) Volcano plot of differentially expressed genes (red, upregulated; blue, downregulated) with adjusted p (padj) <0.05 in naive B cells from (Figure S3A).

(B) Bar plots of the top enriched GO biological processes in healthy and tumor-educated naive B cells.

(C) Bar plots of the top enriched GO biological processes in healthy and tumor-educated naive *BEbi3*$^{-/-}$ cells.

(D) Loading plot overlayed on principal-component analysis (PCA) as derived by differentially expressed gene (DEG) analysis between healthy wild-type (WT), healthy B cell-specific *Ebi3* KO (*BEbi3*$^{-/-}$), tumor-educated WT (WT_tum), and tumor-educated B cell-specific *Ebi3* KO (*BEbi3*$^{-/-}$_tum) naive B cells.

(E) Heatmap of selected differentially expressed genes in naive B cells from healthy or tumor-bearing WT and $B^{EBi3-/-}$ mice. The standardization of log expression was performed by row.

(F) Quantification of intracellular pSTAT3 and Pax5 as determined by flow cytometry in splenic Breg cells isolated from WT mice and activated with αCD40/LPS (Sti, blue) and αCD40/LPS + IL-35 (red) for 48 h.

(G) Quantification of intracellular pSTAT3 (left), Pax5 (middle), and BCL6 (right) analyzed by flow cytometry from intra-tumoral Bcon and Breg.

(H) Relative levels of indicated gene expression in each group, as determined by RNA-seq of peripheral CD19^{+}CD24^{hi}CD38^{hi} Breg or CD19^{+}CD24^{lo}CD38^{lo} B conventiona (Bcon) cells from PDAC patients.

(I) Quantification of IL-35 expression from Breg and Bcon cells isolated from spleens of PDAC patients (n = 25).

(J) The mean fluorescence intensity (MFI) of the intracellular levels of pSTAT3 (left) and Pax5 (right) in Breg and Bcon cells isolated as in (H). Data are representative of three independent experiments. Error bars indicate SEM. NS, non-significant; *p < 0.05; **p < 0.005 (Student's t test, two tailed, unpaired).

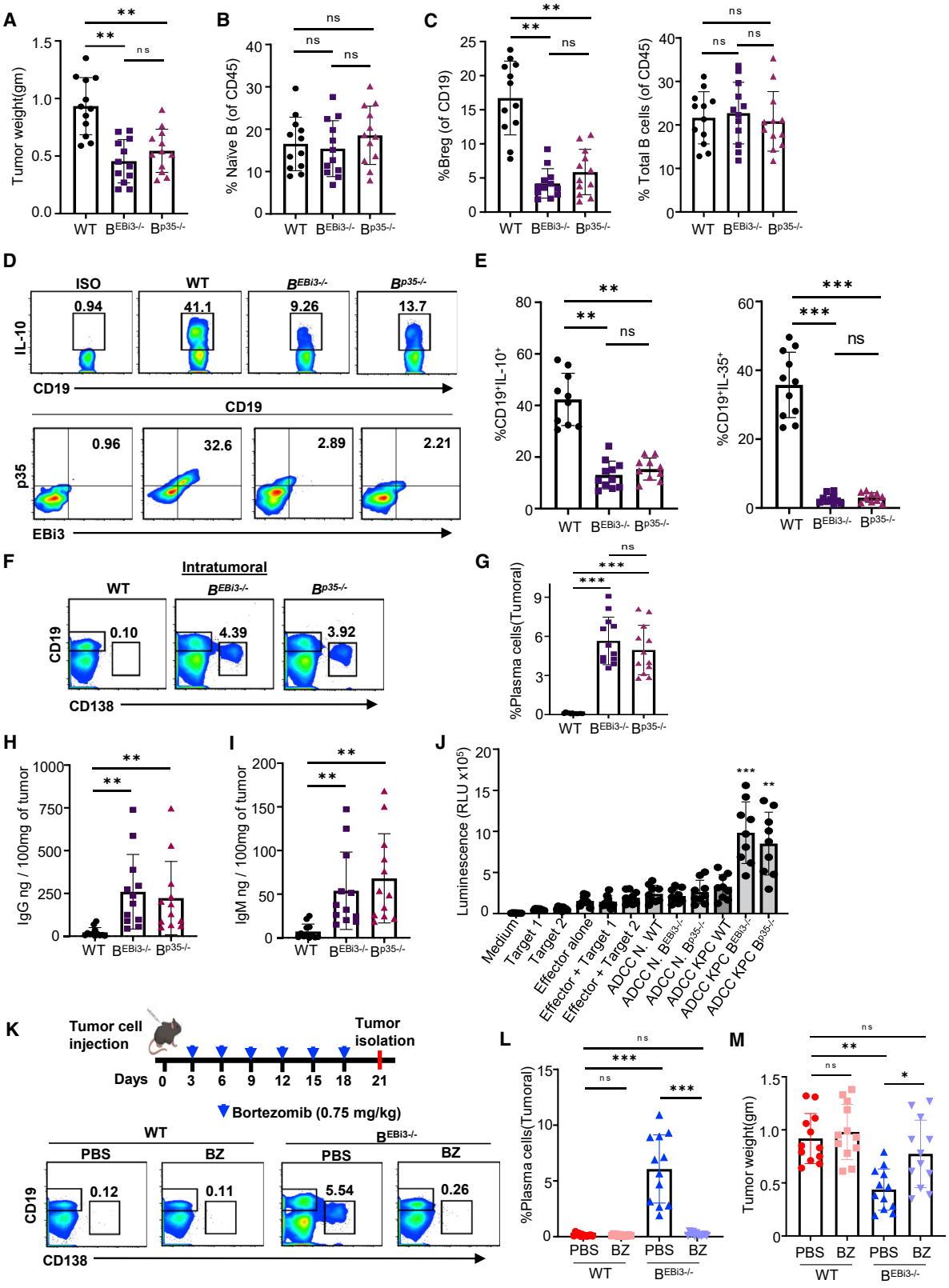

(legend on next page)

which are partially reversed by IL-35 loss with a shift toward plasma cell differentiation features.

Analysis of more terminally differentiated CD21^{hi}CD1d^{hi}CD5^{+} Breg cells confirmed that IL-35 could induce significantly higher levels of pSTAT3 and Pax5 (Figure 2F). Similarly, the intra-tumoral Breg cells isolated from WT mice had higher levels of pSTAT3, Pax5, and BCL6 compared with Bcon cells (Figure 2G). Consistent with murine data, RNA-seq analysis performed on peripheral B cell subsets from PDAC patients[28] revealed significantly increased expression of *BACH1*, *BCL6*, *STAT1*, and *STAT3* and decreased expression of *SDC1* (CD138) gene in CD19^{+}CD24^{hi}CD38^{hi} immunoregulatory IL-35^{+} B cells, compared with conventional B cells (Figures 2H and S3D). As shown previously, this broad subset of B cells also correlated with diminished cytokine upregulation in T cell activation assay (Figures S3E and S3F).[42,43] Consistent with this, we found that CD19^{+}CD24^{hi}CD38^{hi} B cells isolated from resected splenic tissues of PDAC patients had elevated protein level expression of p35, EBi3, pSTAT3, and Pax5 compared with CD19^{+}CD24^{lo}CD38^{lo} conventional B cells (Figures 2I and 2J; n = 25). Together, these data provide evidence that PDAC instructs the upregulation of a transcriptional network consisting of pSTAT3, Pax5, and Bcl6.

IL-35 contributes to B cell dysfunction and suppresses intra-tumoral expansion of plasma cells

To understand how cell-autonomous IL-35 promotes B cell dysfunction in cancer, we analyzed B cell subsets in orthotopic tumor-bearing mice with B cell-specific conditional deletion of IL-35 subunits p35 or Ebi3 ($B^{p35-/-}$ and $B^{EBi3-/-}$ respectively). B cell-specific loss of IL-35 resulted in significant reduction in tumor growth (Figures 3A and S4A).[28] Analysis of intra-tumoral immune cells revealed that IL-35 loss did not significantly alter CD45^{+} leukocyte, and total B cell and naive B cell frequency, but instead specifically decreased the intra-tumoral CD21^{hi}CD1d^{hi}CD5^{+} Breg population (Figures 3B, 3C, S4B–S4D). Production of immunosuppressive cytokines IL-10 and IL-35 by intra-tumoral Breg cells was also significantly reduced compared with WT counterparts (Figures 3D and 3E). On the other hand, consistent with RNA-seq data suggesting a shift toward plasma cell differentiation with loss of IL-35, there was a significant increase in the intra-tumoral proportion of plasma cells in mice with B cell-specific IL-35 deficiency (Figures 3F, 3G, and S4E). Immunoglobulin analysis revealed elevated intra-tumoral immunoglobulin G (IgG) and immunoglobulin M (IgM) antibody isotypes, which inversely correlated with Breg frequency (Figures 3H and 3I). Furthermore, antibody-dependent cellular cytotoxicity assay demonstrated enhanced ability of peripheral effector cells to target tumor cells specifically in the context of IL-35 loss, suggesting antigen-specific recognition (Figure 3J). The frequency of splenic plasma cells in tumor naive $B^{p35-/-}$ and $B^{EBi3-/-}$ mice remained unchanged, suggesting that IL-35 does not regulate plasma cell expansion in a cell-intrinsic manner (Figure S4F). Additional studies using *KPC* cell line 2173 confirmed that B cell-specific loss of IL-35 led increase in accumulation of intra-tumoral plasma cells (Figures S4G–S4K). We previously published that treatment with blocking anti-IL-35 antibody conferred reduction in tumor growth both in spontaneous *KPC* (s*KPC*) and orthotopic models.[28] This treatment also induced intra-tumoral accumulation of plasma cells (Figures S4L–S4O).

To evaluate the functional relevance of plasma cells to pancreatic tumor growth, we used bortezomib, a proteasome inhibitor that can deplete rapidly proliferating auto-reactive plasma cells.[44,45] WT and $B^{EBi3-/-}$ mice were orthotopically injected with *KPC* cells and treated with bortezomib (0.75 mg/kg) or control (Figure 3K). Of note, bortezomib did not alter viability of *KPC4662* cells *in vitro* or affect frequency of T cells, total B cells, and myeloid cell lineages (Figures S5A–S5D). Treatment with bortezomib selectively reduced intra-tumoral plasma cell frequency and rescued tumor growth in $B^{EBi3-/-}$ mice (Figures 3L and 3M). As expected, reduced Breg function via loss of Ebi3 led to an increase in intra-tumoral T cell infiltration (Figures S5E–S5G). This was not affected by plasma cell depletion, suggesting that IL-35 independently affects frequency of effector B and T cells. These data reveal that IL-35 contributes to dysfunctional B cell differentiation by both supporting Breg specification and by restricting tumor-reactive plasma cell expansion in PDAC. Thus, B cell effector function may be actively suppressed in PDAC.

Tumor-educated naive B cells are primed for dysfunction

To better understand how IL-35 may be altering B cell differentiation programs, we examined the differences in response of

Figure 3. IL-35 drives imbalance of plasma and Bregs in cancer

(A) Quantification of tumor weights from WT, $B^{EBi3-/-}$, and $B^{p35-/-}$ mice orthotopically injected with *KPC* cells and collected at 3 weeks post injection. Control WT mice represent both $B^{EBi3+/-}$ and B^{WT} control bone marrow chimera groups.

(B and C) (B) Frequency of intra-tumoral naive B cells (percentage of CD45), and (C) CD21^{hi}CD1d^{hi}CD5^{+} Breg cells (percentage of CD19) and total B cells (percentage of CD45) from Figure 3A as determined by flow cytometry.

(D) Representative flow cytometry plots and (E) quantification of frequency of IL-10, and IL-35 expressing Breg cells from Figure 3A.

(F and G) (F) Representative flow cytometry plots and (G) quantification of CD19^{lo}CD138^{hi} intra-tumoral plasma cells from (A).

(H and I) (H) Quantification of IgG and (I) IgM levels in tumors of WT, $B^{EBi3-/-}$, and $B^{p35-/-}$ mice 3 weeks post orthotopic injection with *KPC* cells.

(J) Representative antibody-dependent cellular cytotoxicity (ADCC) assay for determination of antibody mediated killing of tumor cells (target cells). Target 1, non-cancerous pancreatic cells; target 2, tumor cells (*KPC 4662*); ADCC, effector cells + target cells + source of antibodies (serum samples) from tumor-bearing WT, $B^{EBi3-/-}$, and $B^{p35-/-}$ mice. RLU, relative luminescence units.

(K) Schematic of treatment schedule. Representative flow cytometry plots of intra-tumoral CD19^{lo}CD138^{hi} plasma cells from bortezomib (BZ) or control PBS-treated WT and $B^{EBi3-/-}$ mice 3 weeks post orthotopic injection with *KPC* cells.

(L) Quantification of intra-tumoral CD19^{lo}CD138^{hi} plasma cells from (K).

(M) Quantification of pancreatic tumor weights from (K). Error bars indicate SEM; p values in (A)–(I) were calculated using one-way ANOVA. p values in (J) were calculated using Student's t test, two tailed, unpaired. p values in (L) and (M) were calculated using two-way ANOVA. NS, non-significant; *p < 0.05; **p < 0.005; ***p < 0.001. Data are representative of three independent experiments.

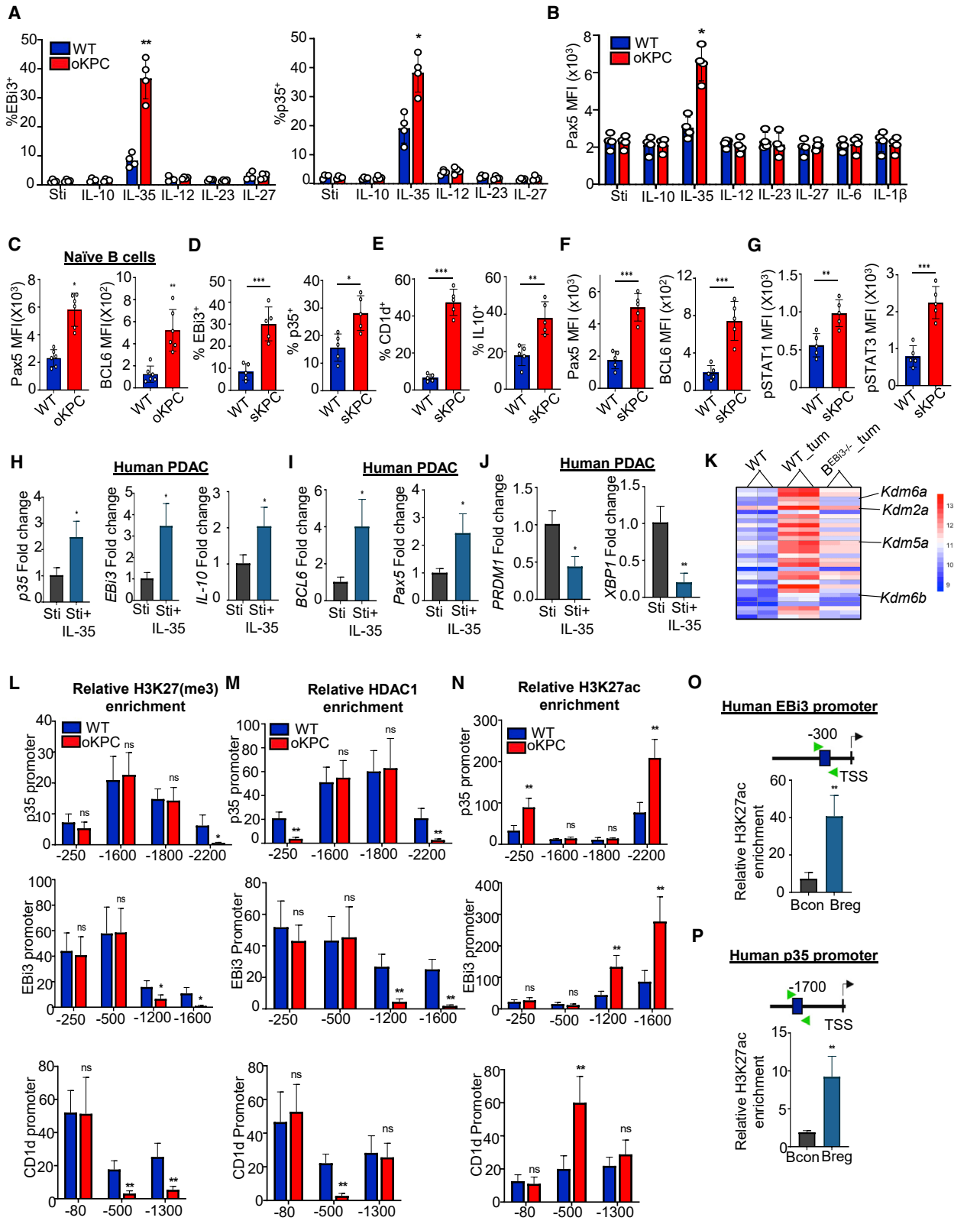

(legend on next page)

naive B cells from healthy or tumor-bearing mice to IL-35 stimulation. Treatment of splenic naive B cells isolated from o*KPC* mice with LPS/αCD40 and rIL-35 induced significantly stronger expression of p35, EBi3, IL10, and CD1d (Figures 4A and S6A). This effect was specific to IL-35 and was not observed with other tested IL-12 family cytokines or IL-10. Flow cytometry analyses confirmed that regulatory cytokine genes, transcriptional regulators Pax5, BCL6, and activated Stat1 and Stat3 were preferentially enriched in LPS/αCD40/rIL-35-treated naive B cells isolated from o*KPC* and s*KPC* mice (Figures 4B–4G and S6B–S6D). Patient-derived splenic naive B cells were also able to respond to rIL-35 treatment by increasing expression of *p35*, *EBi3*, *IL-10*, *Pax5*, and *BCL6* and downregulating *PRDM1* and *XBP1* (Figures 4H–4J). IL-35-driven phenotype persisted in Breg cells, as it induced significantly higher levels of Pax5 (Figure S4E). Similarly, the intra-tumoral Breg cells isolated from WT mice had higher levels of pSTAT3, Pax5, and BCL6 compared with Bcon cells, and this effect was lost with IL-35 deficiency (Figure S6F). Thus, our data reveal that IL-35 not only promotes its own expression, as shown by studies in autoimmune models,[21,39,46,47] but has a broad role in modulating a dysfunctional B cell state characterized by expression of immunosuppressive markers, enrichment of Pax5 and Bcl6, and suppression of plasma cell specifying transcription factors.

We next investigated the mechanism of transcriptional regulation by IL-35. Evaluation of RNA-seq data in naive B cells (Figure 2), revealed significant changes in expression of chromatin and DNA modifiers that were largely alleviated with IL-35 loss (Figure 4K). In particular, several lysine demethylases were significantly upregulated in tumor-educated naive B cells. To assess whether treatment with IL-35 could modulate chromatin modifications and transcription factor enrichment, we performed *in silico* analysis of consensus STAT recognition motifs using TFBIND, TFSEARCH, and PROMO-ALGGEN[48] and identified potential binding sites within the *p35*, *EBi3*, and *Cd1d* promoter regions (Figure S6G). Indeed, we observed a decrease in repressive mark H3K27 trimethylation, reduced HDAC1 recruitment, and increased H3K27 acetylation at the STAT-binding sites in tumor-educated naive B cells (Figure 4L–4N). The H3K27ac mark was similarly enriched at STAT3 consensus binding sites within the *p35* and *EBi3* genes in Breg cells isolated from PDAC patients (Figures 4O and 4P). Tumor-educated naive B cells derived from o*KPC* or s*KPC* mice, compared with healthy controls, were significantly more enriched for pSTAT1 and/or pSTAT3 binding at multiple sites within the *p35*, *EBi3*, and *CD1d* gene promoters (Figures S6H–S6K). Thus, in tumor-educated B cells, IL-35 alters the expression of chromatin regulatory factors, and its effects on target loci are associated with significant changes in chromatin modification state.

IL-35 drives STAT3-Pax5 co-recruitment in tumor-educated B cells

To clarify the mechanism of Pax5 and Bcl6 transcriptional upregulation in tumor-educated naive B cells, we analyzed the *Pax5* and *Bcl6* gene promoters for pSTAT1/3 binding (Figures 5A and 5B). Analysis by chromatin immunoprecipitation (ChIP) showed preferential enrichment of pSTAT3, but not pSTAT1, at the *Pax5* promoter region in tumor-educated naive B cells isolated from o*KPC* and s*KPC* mice (Figures 5C and S7A). pSTAT3 and Pax5 were also both enriched at *Bcl6* promoter in tumor-educated naive B cells compared with WT controls (Figures 5D, 5E and S7B). Using proximity ligation assay (PLA), we discovered that rIL-35, but not rIL-10, rIL-12, rIL-23, and rIL-27, can specifically induce interaction of STAT3 and Pax5 in tumor-educated naive B cells (Figure 5F). Pax5 and STAT3 interaction was lost upon B cell-specific deletion of IL-35 (Figure 5G). ChIP-re-ChIP using double pull-down with pSTAT3 and Pax5 antibodies also confirmed that the STAT3-Pax5 complex binds to the *Bcl6* gene promoter (Figures 5H and S7C). Pax5 had a similar binding pattern to pSTAT3 in naive B cells within the gene promoter regions of *p35*, *EBi3*, and *CD1d*, and exposure to rIL-35 strongly favored enrichment of Pax5 in tumor-educated B cells from o*KPC* and s*KPC* mice (Figures S7D–S7I). Indeed, we observed significant enrichment for co-recruitment of STAT3/Pax5 complex at the promoters of regulatory genes in tumor-educated naive B cells (Figures 5I–5K and S7J–S7L). The STAT3-Pax5 binding sites were important for driving transcription of regulatory genes, as deletion of STAT3-Pax5 binding sequences at sites −2,200 (*p35*), −1600 (*EBi3*), and −500 (*Cd1d*) resulted in decreased luciferase activity in 293T cells upon STAT3 activation (Figures S7M−S7O). These results indicate that formation of a pSTAT3-Pax5 complex is a specific mechanism for transcriptional modulation by IL-35 and may underlie the transcriptional dysregulation of B cell differentiation in PDAC.

Figure 4. Tumor-educated naive B cells are primed for dysfunction

(A) Intracellular levels of EBi3 and p35 in naive B cells from WT and orthotopic *KPC* (o*KPC*) mice treated with LPS/αCD40 ± indicated cytokines for 72 h as determined by flow cytometry.

(B) Intracellular levels of Pax5 in naive B cells from WT and o*KPC* mice treated as in (A) were determined by flow cytometry.

(C) Intracellular levels of Pax5 and BCL6 in LPS/αCD40/rIL-35 treated naive B cells isolated from WT and o*KPC* mice as determined by flow cytometry.

(D–G) (D) Expression of Ebi3 and p35, (E) CD1d and IL-10, (F) Pax5 and Bcl6, and (G) pSTAT1 and pSTAT3 in naive B cells from WT and spontaneous *KPC* (s*KPC*) mice treated as in (A) were determined by flow cytometry.

(H–J) (H) Fold change in expression of *P35*, *EBI3*, *IL10*; (I) *BCL6* and *PAX5*; and (J) *PRDM1* and *XBP1* from naive B cells isolated from spleens of PDAC patients and activated with αCD40/LPS ± rIL-35.

(K) Heatmap of top 30 differentially expressed chromatin and DNA modifiers, fold expression is indicated.

(L–N) (L) Relative H3K27 methylation, (M) HDAC1, and (N) H3K27 acetylation enrichment as determined by ChIP assay at *p35*, *EBi3*, and *Cd1d* gene promoters. Naive B cells isolated from WT (blue) and o*KPC* (red) mice were treated with αCD40/LPS and rIL-35 for 72 h then used for downstream ChIP analysis.

(O and P) (O) Relative H3K27 acetylation enrichment as determined by ChIP assay at *EBI3*, and (P) *P35* gene promoters from Breg and Bcon cells isolated from spleens of PDAC patients. Data are representative of three independent experiments. Error bars indicate SEM. NS, non-significant, *p < 0.05, **p < 0.01, ***p < 0.005 (Student's t test, two tailed, unpaired).

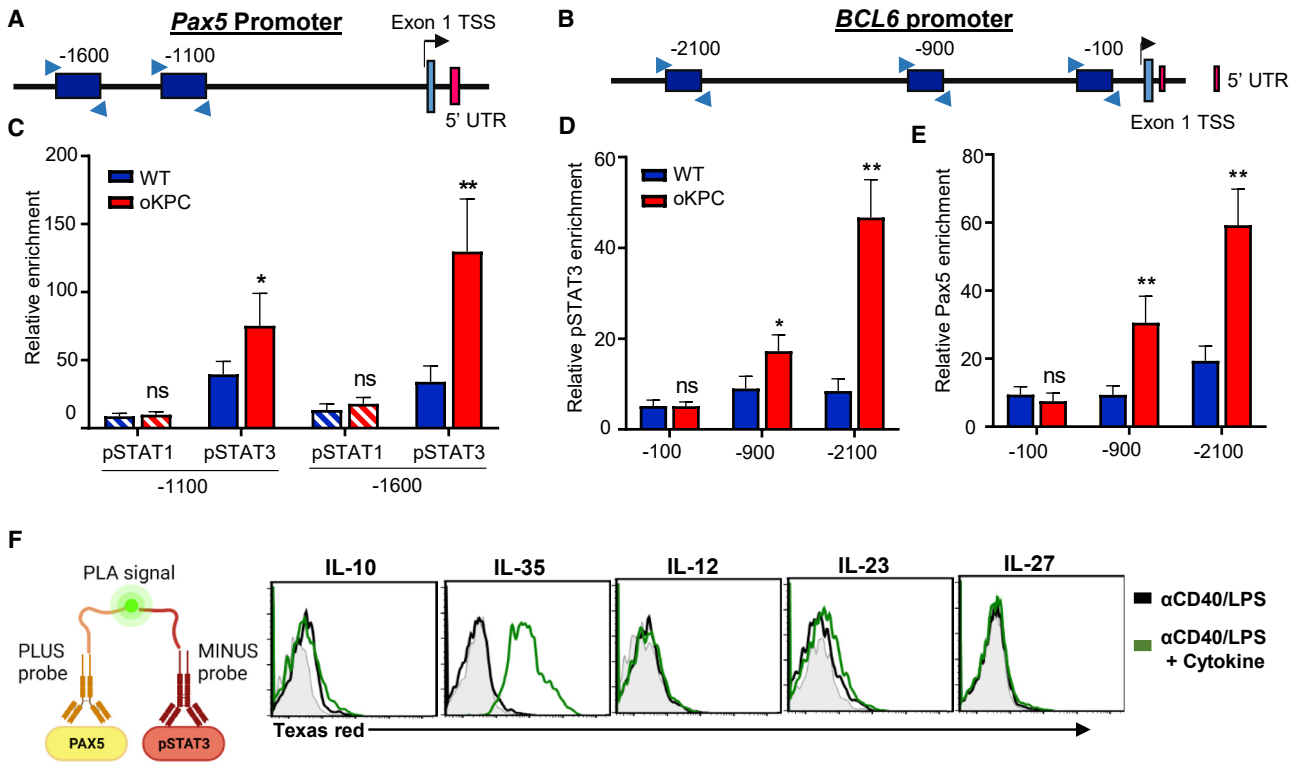

(legend on next page)

IL-35-STAT3 axis deregulates naive B cells in pancreatic cancer

To examine the functional consequences of STAT1/3 regulation on PDAC-associated B cell function, tumor-educated splenic naive B cells were treated with LPS/αCD40/rIL-35 and a STAT1 or STAT3 inhibitor (fludarabine and STA-21, respectively) (Figure S8A). The STAT1 and STAT3 inhibitor did not alter proliferation or viability of naive or Breg cells (Figures S8B and S8C). Inhibition of STAT3, but not STAT1, significantly reduced expression of p35, EBi3, CD1d, Pax5, and Bcl6, whereas IL10 was regulated by both STAT1 or STAT3, suggesting that IL-35/STAT3 exerts a dominant role in specifying IL-35$^+$ Breg cell fate (Figures 6A–6D). Furthermore, inhibition of STAT3, but not STAT1, reduced acetylation levels and Pax5 recruitment at *p35*, *EBi3*, and *Cd1d* gene promoters in tumor-educated naive B cells, indicating that STAT3 is required for IL-35-mediated increases in chromatin modification and Pax5 recruitment at these regulatory loci (Figures 6E, 6F, and S8D–S8I).

To determine whether STAT3 was required for naive B cell dysfunction in PDAC, naive B cells from tumor-bearing mice were treated with LPS/αCD40/rIL-35 and a STAT1 or STAT3 inhibitor and adoptively transferred to B cell-deficient μMT mice (Figure 6G). Three weeks post orthotopic injection of *KPC* cells, inhibition of STAT3, but not STAT1, in B cells significantly reduced tumor burden, decreased Breg frequency and cytokine production, and enhanced intra-tumoral accumulation of plasma cells (Figures 6H–6K and S8J–S8L). Inhibition of STAT3 in B cells also reduced intra-tumoral Treg frequency and enhanced intra-tumoral activity of CD4$^+$ effector cells and cytotoxic CD8$^+$ T cells (Figures S8M−S8P). These data indicate that STAT3 is essential for maintaining immunosuppression of naive B cells in PDAC and that targeting STAT3 is sufficient to induce anti-tumor plasma B cells.

BCL6 expression in tumor-educated naive B cells is required to maintain Breg/plasma cell balance

To examine how upregulation of the transcription factor Bcl6 controls B cell differentiation in PDAC, we treated tumor-educated activated naive B cells with the Bcl6 inhibitor 79-6 (Bcl6i) (Figure 7A).[49] Treatment with the Bcl6 inhibitor did not alter proliferation and viability of naive or Breg cells (Figures S9A and S9B). Adoptive transfer of Bcl6i-treated naive B cells to *μMT* mice resulted in inhibition of tumor growth, accompanied by decreases in intra-tumoral Breg frequency and cytokine production, as well as enhanced intra-tumoral accumulation of plasma cells (Figures 7B–7E and S9C–S9E). We detected increased intra-tumoral IgG and IgM concentration, which inversely correlated with Breg frequency (Figures 7F and 7G). Furthermore, inhibition of BCL6 resulted in reduced expression of *p35* and *EBi3* in intra-tumoral Bregs but did not affect the expression of *IL-10*, demonstrating that BCL6 could potentiate IL-35$^+$ Breg cell fate (Figure 7H). We also observed a significant increase in the frequency of intra-tumoral CD4$^+$ and CD8$^+$ T cells, likely due to reduction in Breg function (Figure 7I).

Recent studies have suggested that improved B and T cell function are a prerequisite for efficacy of immune checkpoint blockade.[6] We found that treatment of PDAC tumor-bearing animals with anti-PD1 in combination with Bcl6 blockade in naive B cells led to an increased frequency of intra-tumoral CD8$^+$ T cells and significantly reduced tumor growth (Figures 7J and 7K). Depletion of CD8$^+$ T partially rescued tumor growth and did not alter plasma cell frequency, suggesting that T cell- and B cell-directed targeting of the tumor may be additive (Figures 7L and S9F–S9I). These results demonstrate that adoptive transfer of tumor-educated naive B cells after BCL6 inhibition is sufficient to reprogram B cell-mediated anti-tumor immune responses and overcome resistance to anti-PD1 immune checkpoint inhibitor therapy in PDAC.

DISCUSSION

Many types of solid malignancies, including pancreatic cancer, select for robust interactions between tumor cells and host responses that establish markedly immunosuppressive environment with influx of myeloid cells, Treg cells, activation of cancer-associated fibroblasts, and expansion of regulatory T and B cell responses.[16,50–53] The balance between regulatory and plasma B cells in the tumor immune microenvironment could determine the sensitivity to immune checkpoint inhibitors, yet the mechanisms that govern B cell differentiation in the context of tumorigenesis are poorly characterized. We discovered that B cells can be derailed from their normal effector function at the naive B cell stage, even in the presence of tumor-specific antigens. Specifically, IL-35/STAT3 signaling axis shifts naive B cells away from plasma cell differentiation and toward regulatory function by stabilizing interaction between pioneer factor Pax5 and pStat3. Genetic or pharmacologic inhibition of the IL-35/STAT3/Bcl6 signaling axis promotes the intra-tumoral accumulation of plasma B cells, affecting tumor growth and resistance to immunotherapy. We propose that transcriptional reprogramming of naive B cells in PDAC could be explored for therapeutic potential.

Figure 5. IL-35 drives STAT3-Pax5 co-recruitment in tumor-educated B cells

(A) Mouse *Pax5* gene promoter with the STAT-binding consensus sites.

(B) Mouse *Bcl6* gene promoter with the STAT and Pax5 binding consensus sites.

(C) ChIP analysis for enrichment of pSTAT1 and pSTAT3 on *Pax5* promoter in naive B cells (treated with αCD40/LPS/rIL-35 for 72 h) from WT or oKPC mice.

(D and E) (D) ChIP analysis for enrichment of pSTAT3 and (E) Pax5 at *Bcl6* promoter from naive B cells isolated and treated as in (C).

(F) Representative flow cytometry plot of Duolink proximity ligation assay (PLA) between pSTAT3 and Pax5 in naive B cells treated with LPS/αCD40/cytokine (green) or LPS/αCD40 alone.

(G) Representative flow cytometry plot of PLA between pSTAT3 and Pax5 in intra-tumoral Breg (green) and Bcon (black) cells.

(H) ChIP-re-ChIP analysis to detect STAT3-Pax5 complex (STAT3:S3, Pax5:P5) at *Bcl6* promoter in rIL-35-treated naive B cells isolated from WT and o*KPC* mice.

(I–K) (I) ChIP-re-ChIP analysis to detect STAT3-Pax5 complex (STAT3:S3, Pax5:P5) at promoters of *p35*, (J) *EBi3*, and (K) *Cd1d* genes in rIL-35-treated naive B cells isolated from WT or o*KPC* mice. Error bars indicate SEM; p values were calculated using two-tailed; unpaired, Student's t test. NS, non-significant, *$p < 0.05$, **$p < 0.005$. Data represent triplicates within the same experiment and are representative of three independent experiments.

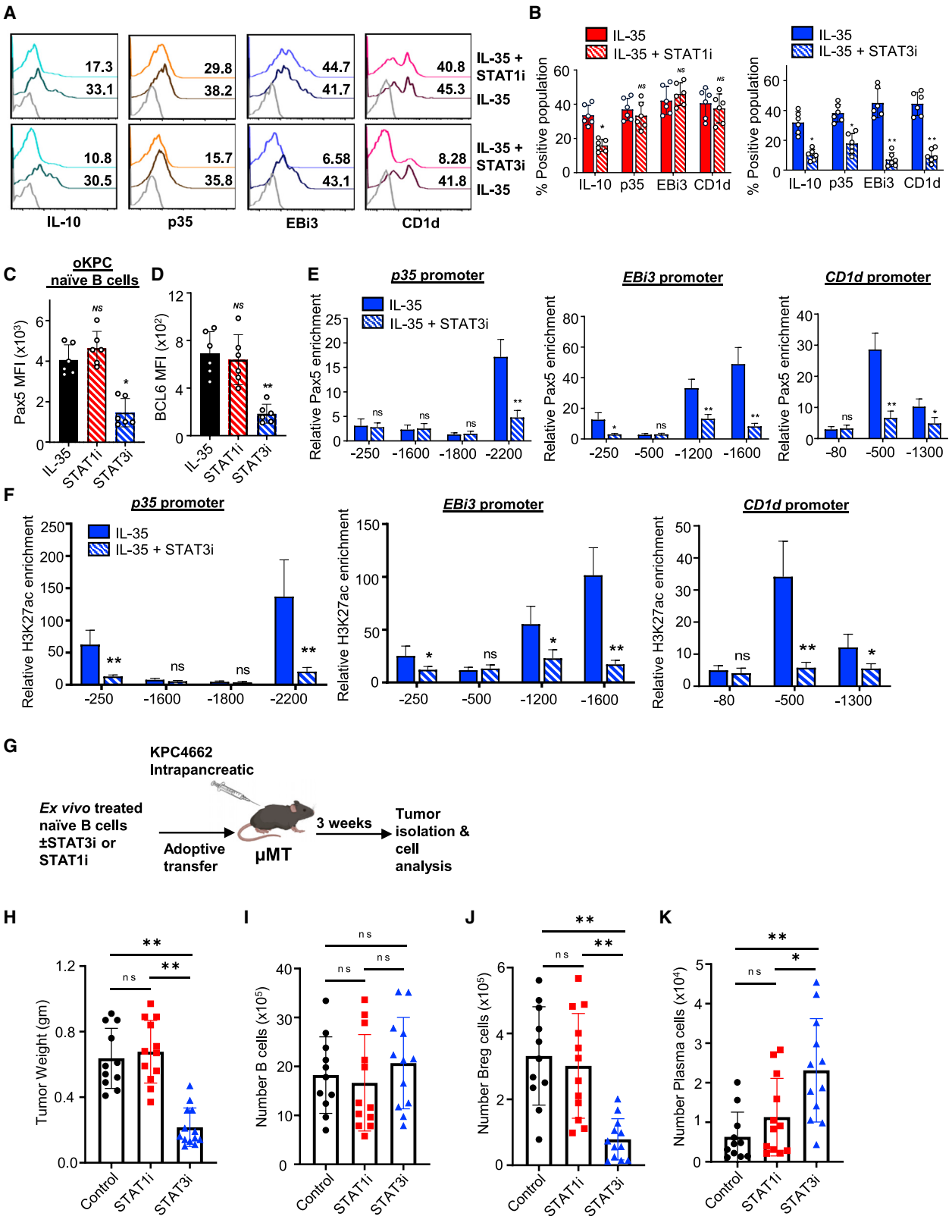

(legend on next page)

We demonstrate that B cell dysfunction in cancer may be an outcome of an active suppression program (mediated by IL-35 as one example) that occurs during tumorigenesis. While prior reports suggest that IL-35 may be able to signal to total B cells in a cell-autonomous manner,[17,21,54] we demonstrate that IL-35 is one of the factors driving B cell dysfunction in cancer and test strategies to reprogram non-reactive tumor-specific B cells to reinvigorate effector cells. Our data show that IL-35 signaling in tumor-educated naive B cells drives interaction between activated Stat3 and pioneer factor Pax5. It is possible that this complex recruits histone modifiers, accounting for changes in observed acetylation and methylation pattern.[55] Recent findings that Pax5 repression alone is unable to activate plasma cell differentiation emphasize the importance of IL-35-induced BCL6 regulation in limiting plasma cell differentiation.[56] Interestingly, a recent finding by Xiao et al. described a role for Bcl6$^+$ Bregs in hepatoma, where expression of Bcl6 was regulated by activation of TLR4, although it is not clear if this contributed to suppression of B cell driven anti-tumor immunity.[19] Nevertheless, diverse additional mechanisms may contribute to stabilization of Pax5, pStat3, and/or Bcl6 expression in naive and other B cell subsets, ultimately contributing to suppression of plasma cell responses in cancer.

Intriguingly, IL-12 family cytokines such as IL-27 and IL-23 and cytokines required for plasma cell activity, such as IL-21 and IL-6, are also potent STAT3 activators.[57,58] Concordantly, cytokines IL-21, IL-4, and IL-6 can induce and stabilize expression of Blimp1 and XBP1 to promote plasma cell differentiation.[59–61] Therefore, while STAT3 activation is required, it is not sufficient for B cell dysfunction elicited by IL-35. Timing of STAT3 activation, additional co-factors, and a primed epigenetic landscape may also play a role.[62]

Our understanding of how plasma cells may contribute to decreased tumor burden requires further investigation. We did not observe IL-35 or IL-10 production by plasma cells in PDAC, potentially due to early reprogramming of naive B cells in our models.[28] However, diverse phenotypic subsets of Bregs have been reported in the literature, including reports of IL-10$^+$ and or IL-35$^+$ plasma cells, suggesting that terminal plasma cell differentiation does not universally present a barrier to subsequent immunosuppressive cytokine production.[17,63,64] It is still not clear whether intra-tumoral plasma cell expansion is mediated locally by tumor neo-antigens or by increased migration and/or homing of B cells that are otherwise engaged systemically.[65] It is also possible that the quality of antibodies produced by newly expanded plasma cells is distinct from the IgGs that can polarize macrophages in PDAC and may contribute to destruction of cancer cells via tumor cell lysis.[7,66,67] Understanding clonal distribution of B cells and Breg cells before and after IL-35 loss may also elucidate the selection of B cell antigenic responses that contribute to PDAC growth. Intra-tumoral effector B cells may also directly or indirectly contribute to maturation of tertiary immune structures and support T cell immunity.[4,5,68,69] Deconvolution of these putative plasma B cell-driven mechanisms of action will enable the design of appropriate combination immunotherapies that can synergize with effector B cell reprogramming for better control of tumor growth. Further studies using genetic models of selective reduction in antibody production (AID/μS knockout [KO]), and/or Stat3 inactivation and passive transfer of antibodies will allow us to discern the contribution of newly generated antibody response to PDAC rejection, while circumventing potential off-target effects of small-molecule inhibitors.[70]

Cancer-derived factors that contribute to B cell dysfunction are not yet clear. Possible candidate factors include antigenic determinants, such as variability of antigen strength and/or timing of tumor-associated antigen exposure. Damage-associated molecular patterns may also be systemically elevated by PDAC, and can modulate B cell biology.[71,72] Microbial contexture is likely to be of particular importance and interest, especially given the known presence of bacterial components in PDAC tumors and the general propensity of PDAC patients to experience gut dysbiosis.[73–76] Our findings suggest that pathologic reprogramming of naive B cells in PDAC may be reversible. Further exploration of mechanisms that underlie Breg cell lineage commitment may reveal therapeutic strategies that enhance plasma cell function in cancer and synergize with T cell-directed immunotherapies.

Limitations of the study

Although our study utilizes both human and mouse B cell profiling, B cell subsets were enriched for their ability to produce immunosuppressive cytokines. It should be noted that identifying/streamlining functional subsets of B cells based on transcriptomics, function, and localization will be necessary to further discern potential prognostic value in both patients and

Figure 6. IL-35-STAT3 axis deregulates naive B cells in pancreatic cancer

(A) Representative flow cytometry histogram plot of intracellular IL10, p35, EBi3, and surface CD1d in naive B cells isolated from o*KPC* mice and treated as indicated.

(B) Quantification of IL10, p35, EBi3, and CD1d in naive B cells treated as in (A), with STAT1 inhibitor (left) and STAT3 inhibitor (right).

(C) Quantification of Pax5 in naive B cells treated as in (A).

(D) Quantification of Bcl6 in naive B cells treated as in (A).

(E) ChIP analysis for enrichment of Pax5 at *p35*, *EBi3*, and *Cd1d* gene promoters. Naive B cells isolated from o*KPC* mice were treated with αCD40/LPS and ± STAT3 inhibitor for 72 h followed by ChIP analysis.

(F) ChIP analysis for enrichment of H3K27ac at *p35*, *EBi3*, and *Cd1d* gene promoters. Naive B cells were isolated and treated as in (E).

(G) Experimental schematic used to investigate *in vivo* effect of STAT1 (STAT1i) and STAT3 (STAT3i) inhibition in B cells on pancreatic tumor growth.

(H) Quantification of tumor weights from mice in (G).

(I) Absolute number of intra-tumoral B cells from mice in (H).

(J) Absolute number of intra-tumoral Breg cells from mice in (H).

(K) Absolute number of intra-tumoral plasma cells from mice in (H). Error bars indicate SEM; p values were calculated using two-tailed; unpaired, Student's t test. p values in (H) to (K) were calculated using one-way ANOVA. NS, non-significant, *$p < 0.05$, **$p < 0.005$. Data are representative of three independent experiments.

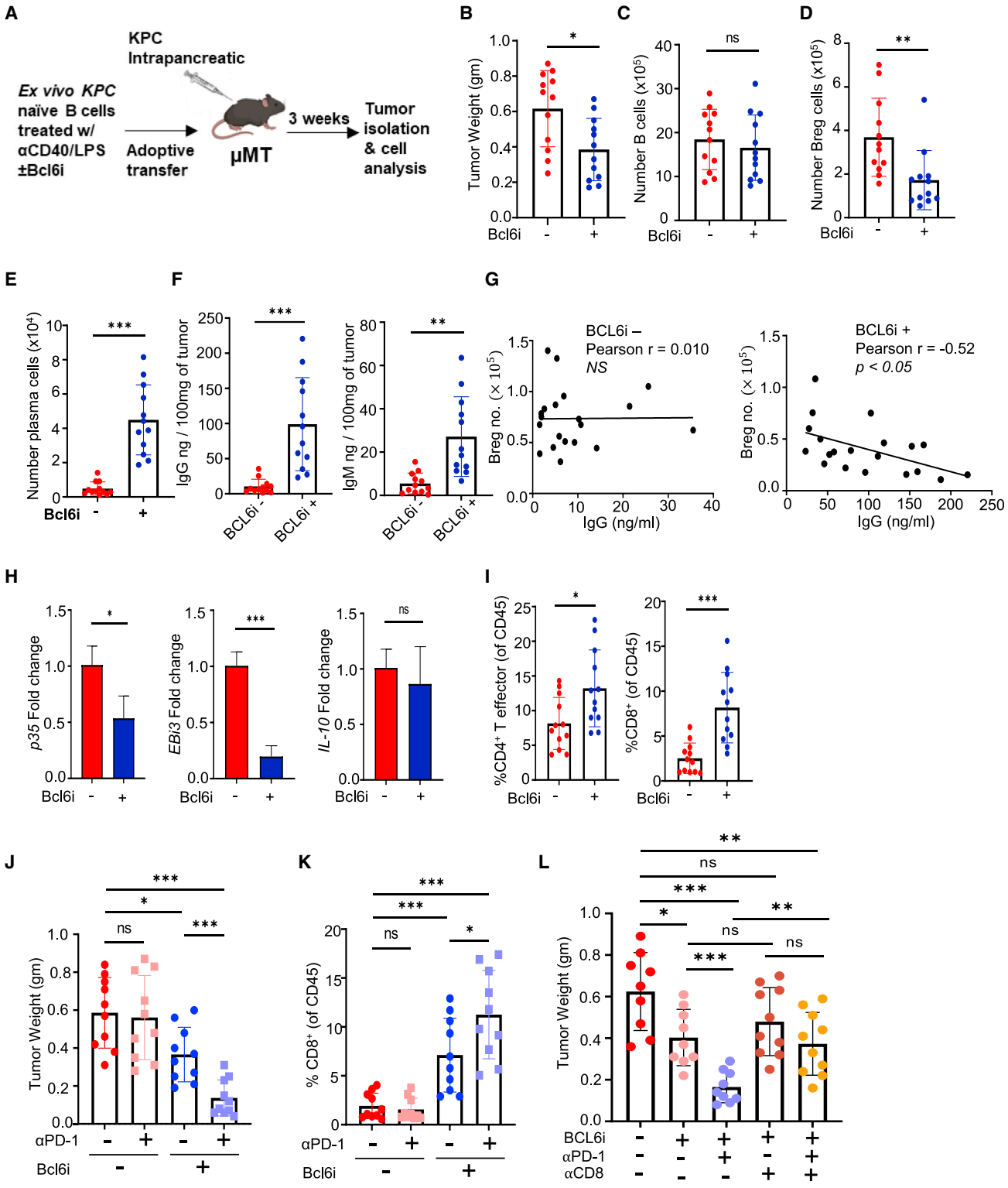

Figure 7. BCL6 inhibition in tumor-educated naive B cells restrains tumor growth

(A) Experimental schematic used to test *in vivo* effect of Bcl6 inhibition (Bcl6i) in B cells on pancreatic tumor growth. Naive B cells from o*KPC* mice were treated with αCD40/LPS/IL-35 ± Bcl6i and transferred into *μMT* mice, followed by orthotopic injection of *KPC* cells.

(B) Quantification of tumor weights from *μMT* mice as in (A).

(C–E) (C) Absolute number of intra-tumoral B cells, (D) Breg cells, and (E) plasma cells in mice from (B).

(legend continued on next page)

mouse models. Our study utilized mouse cancer cell lines and a spontaneous $Kras^{G12D}$;$P53^{R172H}$-driven model of pancreatic cancer. It is of note that these models are characterized by marked immunosuppression and have limited neoantigen pool; therefore, analysis of additional cell lines and/or more immunogenic models of cancer would be important to understand the full scope of B cell functionality in solid cancers. Furthermore, studies utilizing patient-derived data will lead to better understanding of human-specific nuances of the B cell responses in cancer that are otherwise difficult to model using animal systems.

STAR★METHODS

Detailed methods are provided in the online version of this paper and include the following:

- KEY RESOURCES TABLE
- RESOURCE AVAILABILITY
  - Lead contact
  - Materials availability
  - Data and code availability
- EXPERIMENTAL MODEL AND SUBJECT DETAILS
  - Mice
  - Cell lines
  - Human samples
  - Primary lymphocyte cells
  - *In vitro* culture of primary B and T cells
- METHOD DETAILS
  - Bone marrow mouse chimera generation
  - Mouse tumor cell injection studies
  - Mouse tumor treatment studies
  - Lymphocyte isolation
  - Breg and Bcon cell isolation from human spleen
  - MTT assay
  - B cell: T cell co-culture
  - *In vitro* treatment and adoptive transfer of B cells
  - Intracellular cytokine and transcription factor staining
  - ChIP and ChIP-re-ChIP
  - QPCR analysis for gene expression
  - Proximity ligation assay
  - RNAseq library preparation and analysis
  - Luciferase reporter assay
  - Enzyme-linked immunosorbent assay (ELISA)
  - Antibody-dependent cellular cytotoxicity (ADCC)
  - Depletion of $CD8^+$ T cells, and αIL-35 treatment *in vivo*
  - Immunohistochemistry
  - Immunofluorescence on human tissues
  - Human immunoregulatory B cell signature
- QUANTIFICATION AND STATISTICAL ANALYSIS

SUPPLEMENTAL INFORMATION

Supplemental information can be found online at https://doi.org/10.1016/j.xcrm.2022.100744.

ACKNOWLEDGMENTS

We thank G.P. Gupta, X. Peng, A. Tsagaratou, and G. Dotti for discussions and help with manuscript preparation, and C. Steward, H. Kelkar, and N. Kren for help with proofreading and IPA analysis. Funding: this work was supported by R37 CA230786 (Y.P.-G.), University Cancer Research Fund at the UNC Chapel Hill (Y.P.-G. and W.Y.K.), V Foundation for Cancer Research grant V2016-016 (Y.P.-G.), Concern Foundation Conquer Cancer Now Award (Y.P.G), and R35 CA232109 (J.P.-Y.T.). The UNC Flow Cytometry Core Facility, Translational Pathology Laboratory, Animal Histopathology & Laboratory Medicine Core, and the UNC Lineberger Animal Studies Core are supported in part by P30 CA016086 Cancer Center Core Support Grant to the UNC LCCC. Bioinformatics and Analytics Research Collaborative is supported by UNC School of Medicine strategic funds. Some illustrations in the figures were made using BioRender.

AUTHOR CONTRIBUTIONS

Conceptualization, original hypothesis, and design of the study, B.M. and Y.P.-G; methodology, B.M., Y.W., S.L., C.H., A.M., and Y.P.-G.; investigation, B.M., Y.W., T.D.B, S.L., M.Z., S.E., and Y.P.-G; writing – original draft, B.M. and Y.P.-G; writing – review & editing, all authors; resources, G.H., B.G.V., J.P.-Y.T., N.R., W.Y.K., and J.J.Y.; supervision, W.Y.K., J.J.Y., B.G.V., and Y.P.-G.

DECLARATION OF INTERESTS

B.G.V. declares equity in GeneCentric Therapeutics.

Received: July 1, 2021
Revised: June 30, 2022
Accepted: August 23, 2022
Published: September 12, 2022

REFERENCES

1. O'Donnell, J.S., Teng, M.W.L., and Smyth, M.J. (2019). Cancer immunoediting and resistance to T cell-based immunotherapy. Nat. Rev. Clin. Oncol. *16*, 151–167.
2. Waldman, A.D., Fritz, J.M., and Lenardo, M.J. (2020). A guide to cancer immunotherapy: from T cell basic science to clinical practice. Nat. Rev. Immunol. *20*, 651–668.
3. Petitprez, F., de Reyniès, A., Keung, E.Z., Chen, T.W.-W., Sun, C.-M., Calderaro, J., Jeng, Y.-M., Hsiao, L.-P., Lacroix, L., Bougoüin, A., et al. (2020).

(F) Quantification of IgG and IgM levels in tumors from mice in (B).
(G) Correlation between intra-tumoral Breg cells and IgG levels from mice in (B).
(H) Fold change in expression of *p35*, *EBi3*, and *IL-10* as determined by qPCR in intra-tumoral Breg cells isolated from mice in (B).
(I) Frequency of intra-tumoral T effector ($CD45^+CD4^+CD25^-$) and cytotoxic T cells ($CD45^+CD8^+$) in mice from (B).
(J) Quantification of tumor weight from *μMT* mice 3 weeks post orthotopic adoptive transfer of pre-treated B cells and intra-pancreatic injections with *KPC* cells as in (A) ± treatment with αPD-1 on days 7, 9, and 11.
(K) Frequency of intra-tumoral cytotoxic T cells ($CD45^+CD8^+$) in mice from (J).
(L) Quantification of tumor weight from *μMT* mice 3 weeks post orthotopic adoptive transfer of pre-treated B cells and intra-pancreatic injections with *KPC* cells as in (J) ± depletion of CD8 T cells. Error bars indicate SEM; p values were calculated using two-tailed, unpaired Student's t test. NS, non-significant, $^*p < 0.05$, $^{**}p < 0.005$, $^{***}p < 0.001$. Data are representative of three independent experiments. Experiments using $CD8^+$ depletion were performed with 7- to 8-week-old *μMT* mice with at least six mice per group in duplicate.

B cells are associated with survival and immunotherapy response in sarcoma. Nature *577*, 556–560.

4. Cabrita, R., Lauss, M., Sanna, A., Donia, M., Skaarup Larsen, M., Mitra, S., Johansson, I., Phung, B., Harbst, K., Vallon-Christersson, J., et al. (2020). Tertiary lymphoid structures improve immunotherapy and survival in melanoma. Nature *577*, 561–565.
5. Helmink, B.A., Reddy, S.M., Gao, J., Zhang, S., Basar, R., Thakur, R., Yizhak, K., Sade-Feldman, M., Blando, J., Han, G., et al. (2020). B cells and tertiary lymphoid structures promote immunotherapy response. Nature *577*, 549–555.
6. Hollern, D.P., Xu, N., Thennavan, A., Glodowski, C., Garcia-Recio, S., Mott, K.R., He, X., Garay, J.P., Carey-Ewend, K., Marron, D., et al. (2019). B cells and T follicular helper cells mediate response to checkpoint inhibitors in high mutation burden mouse models of breast cancer. Cell *179*, 1191–1206.e21.
7. Sharonov, G.V., Serebrovskaya, E.O., Yuzhakova, D.V., Britanova, O.V., and Chudakov, D.M. (2020). B cells, plasma cells and antibody repertoires in the tumour microenvironment. Nat. Rev. Immunol. *20*, 294–307.
8. Clark, C.E., Hingorani, S.R., Mick, R., Combs, C., Tuveson, D.A., and Vonderheide, R.H. (2007). Dynamics of the immune reaction to pancreatic cancer from inception to invasion. Cancer Res. *67*, 9518–9527.
9. Royal, R.E., Levy, C., Turner, K., Mathur, A., Hughes, M., Kammula, U.S., Sherry, R.M., Topalian, S.L., Yang, J.C., and Lowy, I. (2010). Phase 2 trial of single agent Ipilimumab (anti-CTLA-4) for locally advanced or metastatic pancreatic adenocarcinoma. J. Immunother. *33*, 828–833.
10. Brahmer, J.R., Tykodi, S.S., Chow, L.Q.M., Hwu, W.-J., Topalian, S.L., Hwu, P., Drake, C.G., Camacho, L.H., Kauh, J., Odunsi, K., et al. (2012). Safety and activity of anti–PD-L1 antibody in patients with advanced cancer. N. Engl. J. Med. *366*, 2455–2465.
11. Vonderheide, R.H., and Bayne, L.J. (2013). Inflammatory networks and immune surveillance of pancreatic carcinoma. Curr. Opin. Immunol. *25*, 200–205.
12. Feig, C., Gopinathan, A., Neesse, A., Chan, D.S., Cook, N., and Tuveson, D.A. (2012). The pancreas cancer microenvironment. Clin. Cancer Res. *18*, 4266–4276.
13. Wouters, M.C.A., and Nelson, B.H. (2018). Prognostic significance of tumor-infiltrating B cells and plasma cells in human cancer. Clin. Cancer Res. *24*, 6125–6135.
14. Largeot, A., Pagano, G., Gonder, S., Moussay, E., and Paggetti, J. (2019). The B-side of cancer immunity: the underrated tune. Cells *8*, 449.
15. He, Y., Qian, H., Liu, Y., Duan, L., Li, Y., and Shi, G. (2014). The roles of regulatory B cells in cancer. J. Immunol. Res., 215471.
16. Michaud, D., Steward, C.R., Mirlekar, B., and Pylayeva-Gupta, Y. (2021). Regulatory B cells in cancer. Immunol. Rev. *299*, 74–92.
17. Shen, P., Roch, T., Lampropoulou, V., O'Connor, R.A., Stervbo, U., Hilgenberg, E., Ries, S., Dang, V.D., Jaimes, Y., Daridon, C., et al. (2014). IL-35-producing B cells are critical regulators of immunity during autoimmune and infectious diseases. Nature *507*, 366–370.
18. Shen, P., and Fillatreau, S. (2015). Antibody-independent functions of B cells: a focus on cytokines. Nat. Rev. Immunol. *15*, 441–451.
19. Xiao, X., Lao, X.-M., Chen, M.-M., Liu, R.-X., Wei, Y., Ouyang, F.-Z., Chen, D.-P., Zhao, X.-Y., Zhao, Q., Li, X.-F., et al. (2016). PD-1hi identifies a novel regulatory B-cell population in human hepatoma that promotes disease progression. Cancer Discov. *6*, 546–559.
20. Ren, Z., Peng, H., and Fu, Y.-X. (2016). PD-1 shapes B cells as evildoers in the tumor microenvironment. Cancer Discov. *6*, 477–478.
21. Wang, R.-X., Yu, C.-R., Dambuza, I.M., Mahdi, R.M., Dolinska, M.B., Sergeev, Y.V., Wingfield, P.T., Kim, S.-H., and Egwuagu, C.E. (2014). Interleukin-35 induces regulatory B cells that suppress autoimmune disease. Nat. Med. *20*, 633–641.
22. Pylayeva-Gupta, Y., Das, S., Handler, J.S., Hajdu, C.H., Coffre, M., Koralov, S.B., and Bar-Sagi, D. (2016). IL35-producing B cells promote the development of pancreatic neoplasia. Cancer Discov. *6*, 247–255.
23. Yanaba, K., Bouaziz, J.-D., Haas, K.M., Poe, J.C., Fujimoto, M., and Tedder, T.F. (2008). A regulatory B cell subset with a unique CD1dhiCD5+ phenotype controls T cell-dependent inflammatory responses. Immunity *28*, 639–650.
24. Mauri, C., and Bosma, A. (2012). Immune regulatory function of B cells. Annu. Rev. Immunol. *30*, 221–241.
25. Korniotis, S., Gras, C., Letscher, H., Montandon, R., Mégret, J., Siegert, S., Ezine, S., Fallon, P.G., Luther, S.A., Fillatreau, S., and Zavala, F. (2016). Treatment of ongoing autoimmune encephalomyelitis with activated B-cell progenitors maturing into regulatory B cells. Nat. Commun. *7*, 12134.
26. Cherukuri, A., Mohib, K., and Rothstein, D.M. (2021). Regulatory B cells: TIM-1, transplant tolerance, and rejection. Immunol. Rev. *299*, 31–44.
27. Mirlekar, B., Michaud, D., Searcy, R., Greene, K., and Pylayeva-Gupta, Y. (2018). IL35 hinders endogenous antitumor T-cell immunity and responsiveness to immunotherapy in pancreatic cancer. Cancer Immunol. Res. *6*, 1014–1024.
28. Mirlekar, B., Michaud, D., Lee, S.J., Kren, N.P., Harris, C., Greene, K., Goldman, E.C., Gupta, G.P., Fields, R.C., Hawkins, W.G., et al. (2020). B cell–derived IL35 drives STAT3-dependent CD8+ T-cell exclusion in pancreatic cancer. Cancer Immunol. Res. *8*, 292–308.
29. Kroeger, D.R., Milne, K., and Nelson, B.H. (2016). Tumor-infiltrating plasma cells are associated with tertiary lymphoid structures, cytolytic T-cell responses, and superior prognosis in ovarian cancer. Clin. Cancer Res. *22*, 3005–3015.
30. Gupta, P., Chen, C., Chaluvally-Raghavan, P., and Pradeep, S. (2019). B cells as an immune-regulatory signature in ovarian cancer. Cancers *11*, 894.
31. Bosisio, F.M., Wilmott, J.S., Volders, N., Mercier, M., Wouters, J., Stas, M., Blokx, W.A., Massi, D., Thompson, J.F., Scolyer, R.A., et al. (2016). Plasma cells in primary melanoma. Prognostic significance and possible role of IgA. Mod. Pathol. *29*, 347–358.
32. Verma, R., and Kumar, L. (2020). Plasma cells in the melanoma tumor microenvironment—mechanistic roles for IgA. Front. Immunol. *11*, 979.
33. Chen, B., Khodadoust, M.S., Liu, C.L., Newman, A.M., and Alizadeh, A.A. (2018). Profiling tumor infiltrating immune cells with CIBERSORT. Methods Mol. Biol. *1711*, 243–259.
34. Stromnes, I.M., Schmitt, T.M., Hulbert, A., Brockenbrough, J.S., Nguyen, H., Cuevas, C., Dotson, A.M., Tan, X., Hotes, J.L., and Greenberg, P.D. (2015). T cells engineered against a native antigen can surmount immunologic and physical barriers to treat pancreatic ductal adenocarcinoma. Cancer Cell *28*, 638–652.
35. Hingorani, S.R., Wang, L., Multani, A.S., Combs, C., Deramaudt, T.B., Hruban, R.H., Rustgi, A.K., Chang, S., and Tuveson, D.A. (2005). Trp53R172H and KrasG12D cooperate to promote chromosomal instability and widely metastatic pancreatic ductal adenocarcinoma in mice. Cancer Cell *7*, 469–483.
36. Méndez, A., and Mendoza, L. (2016). A network model to describe the terminal differentiation of B cells. PLoS Comput. Biol. *12*, e1004696.
37. Nutt, S.L., Hodgkin, P.D., Tarlinton, D.M., and Corcoran, L.M. (2015). The generation of antibody-secreting plasma cells. Nat. Rev. Immunol. *15*, 160–171.
38. Tarlinton, D., Radbruch, A., Hiepe, F., and Dörner, T. (2008). Plasma cell differentiation and survival. Curr. Opin. Immunol. *20*, 162–169.
39. Dambuza, I.M., He, C., Choi, J.K., Yu, C.-R., Wang, R., Mattapallil, M.J., Wingfield, P.T., Caspi, R.R., and Egwuagu, C.E. (2017). IL-12p35 induces expansion of IL-10 and IL-35-expressing regulatory B cells and ameliorates autoimmune disease. Nat. Commun. *8*, 719.
40. Wang, L., Fu, Y., Yu, B., Jiang, X., Liu, H., Liu, J., Zha, B., and Chu, Y. (2021). HSP70, a novel regulatory molecule in B cell-mediated suppression of autoimmune diseases. J. Mol. Biol. *433*, 166634.

41. Choy, M.S., Yusoff, P., Lee, I.C., Newton, J.C., Goh, C.W., Page, R., Shenolikar, S., and Peti, W. (2015). Structural and functional analysis of the GADD34: PP1 eIF2α phosphatase. Cell Rep. *11*, 1885–1891.

42. Blair, P.A., Noreña, L.Y., Flores-Borja, F., Rawlings, D.J., Isenberg, D.A., Ehrenstein, M.R., and Mauri, C. (2010). CD19+ CD24hiCD38hi B cells exhibit regulatory capacity in healthy individuals but are functionally impaired in systemic lupus erythematosus patients. Immunity *32*, 129–140.

43. Flores-Borja, F., Bosma, A., Ng, D., Reddy, V., Ehrenstein, M.R., Isenberg, D.A., and Mauri, C. (2013). CD19+ CD24hiCD38hi B cells maintain regulatory T cells while limiting TH1 and TH17 differentiation. Sci. Transl. Med. *5*, 173ra23.

44. Alexander, T., Sarfert, R., Klotsche, J., Kühl, A.A., Rubbert-Roth, A., Lorenz, H.-M., Rech, J., Hoyer, B.F., Cheng, Q., Waka, A., et al. (2015). The proteasome inhibitior bortezomib depletes plasma cells and ameliorates clinical manifestations of refractory systemic lupus erythematosus. Ann. Rheum. Dis. *74*, 1474–1478.

45. Neubert, K., Meister, S., Moser, K., Weisel, F., Maseda, D., Amann, K., Wiethe, C., Winkler, T.H., Kalden, J.R., and Manz, R.A. (2008). The proteasome inhibitor bortezomib depletes plasma cells and protects mice with lupus-like disease from nephritis. Nat. Med. *14*, 748–755.

46. Matsushita, T., and Tedder, T.F. (2010). Identifying regulatory B cells (B10 cells) that produce IL-10 in mice. In Suppression and Regulation of Immune Responses (Springer), pp. 99–111.

47. Sun, J., and Basu, U. (2021). Purification of murine IL-10+ B cells for analyses of biological functions and transcriptomics. In Regulatory B Cells (Springer), pp. 307–321.

48. Farré, D., Roset, R., Huerta, M., Adsuara, J.E., Roselló, L., Albà, M.M., and Messeguer, X. (2003). Identification of patterns in biological sequences at the ALGGEN server: PROMO and MALGEN. Nucleic Acids Res. *31*, 3651–3653.

49. Cerchietti, L.C., Ghetu, A.F., Zhu, X., Da Silva, G.F., Zhong, S., Matthews, M., Bunting, K.L., Polo, J.M., Farès, C., Arrowsmith, C.H., et al. (2010). A small-molecule inhibitor of BCL6 kills DLBCL cells in vitro and in vivo. Cancer Cell *17*, 400–411.

50. Helms, E., Onate, M.K., and Sherman, M.H. (2020). Fibroblast heterogeneity in the pancreatic tumor microenvironment. Cancer Discov. *10*, 648–656.

51. Bear, A.S., Vonderheide, R.H., and O'Hara, M.H. (2020). Challenges and opportunities for pancreatic cancer immunotherapy. Cancer Cell *38*, 788–802.

52. Leinwand, J., and Miller, G. (2020). Regulation and modulation of antitumor immunity in pancreatic cancer. Nat. Immunol. *21*, 1152–1159.

53. Jiang, H., Hegde, S., and DeNardo, D.G. (2017). Tumor-associated fibrosis as a regulator of tumor immunity and response to immunotherapy. Cancer Immunol. Immunother. *66*, 1037–1048.

54. Vignali, D.A.A., and Kuchroo, V.K. (2012). IL-12 family cytokines: immunological playmakers. Nat. Immunol. *13*, 722–728.

55. Suan, D., Sundling, C., and Brink, R. (2017). Plasma cell and memory B cell differentiation from the germinal center. Curr. Opin. Immunol. *45*, 97–102.

56. Liu, G.J., Jaritz, M., Wöhner, M., Agerer, B., Bergthaler, A., Malin, S.G., and Busslinger, M. (2020). Repression of the B cell identity factor Pax5 is not required for plasma cell development. J. Exp. Med. *217*, e20200147.

57. Berglund, L.J., Avery, D.T., Ma, C.S., Moens, L., Deenick, E.K., Bustamante, J., Boisson-Dupuis, S., Wong, M., Adelstein, S., Arkwright, P.D., et al. (2013). IL-21 signalling via STAT3 primes human naive B cells to respond to IL-2 to enhance their differentiation into plasmablasts. Blood *122*, 3940–3950.

58. Wan, C.-K., Andraski, A.B., Spolski, R., Li, P., Kazemian, M., Oh, J., Samsel, L., Swanson, P.A., McGavern, D.B., Sampaio, E.P., et al. (2015). Opposing roles of STAT1 and STAT3 in IL-21 function in CD4+ T cells. Proc. Natl. Acad. Sci. USA *112*, 9394–9399.

59. Moens, L., and Tangye, S.G. (2014). Cytokine-mediated regulation of plasma cell generation: IL-21 takes center stage. Front. Immunol. *5*, 65.

60. Nutt, S.L., and Kee, B.L. (2007). The transcriptional regulation of B cell lineage commitment. Immunity *26*, 715–725.

61. Wang, S., Wang, J., Kumar, V., Karnell, J.L., Naiman, B., Gross, P.S., Rahman, S., Zerrouki, K., Hanna, R., Morehouse, C., et al. (2018). IL-21 drives expansion and plasma cell differentiation of autoreactive CD11c hi T-bet+ B cells in SLE. Nat. Commun. *9*, 1758.

62. Hutchins, A.P., Diez, D., Takahashi, Y., Ahmad, S., Jauch, R., Tremblay, M.L., and Miranda-Saavedra, D. (2013). Distinct transcriptional regulatory modules underlie STAT3's cell type-independent and cell type-specific functions. Nucleic Acids Res. *41*, 2155–2170.

63. Shalapour, S., Lin, X.-J., Bastian, I.N., Brain, J., Burt, A.D., Aksenov, A.A., Vrbanac, A.F., Li, W., Perkins, A., Matsutani, T., et al. (2017). Inflammation-induced IgA+ cells dismantle anti-liver cancer immunity. Nature *551*, 340–345.

64. Shalapour, S., Font-Burgada, J., Di Caro, G., Zhong, Z., Sanchez-Lopez, E., Dhar, D., Willimsky, G., Ammirante, M., Strasner, A., Hansel, D.E., et al. (2015). Immunosuppressive plasma cells impede T-cell-dependent immunogenic chemotherapy. Nature *521*, 94–98.

65. Isaeva, O.I., Sharonov, G.V., Serebrovskaya, E.O., Turchaninova, M.A., Zaretsky, A.R., Shugay, M., and Chudakov, D.M. (2019). Intratumoral immunoglobulin isotypes predict survival in lung adenocarcinoma subtypes. J. Immunother. Cancer *7*, 279.

66. Kurai, J., Chikumi, H., Hashimoto, K., Yamaguchi, K., Yamasaki, A., Sako, T., Touge, H., Makino, H., Takata, M., Miyata, M., et al. (2007). Antibody-dependent cellular cytotoxicity mediated by cetuximab against lung cancer cell lines. Clin. Cancer Res. *13*, 1552–1561.

67. Gunderson, A.J., Kaneda, M.M., Tsujikawa, T., Nguyen, A.V., Affara, N.I., Ruffell, B., Gorjestani, S., Liudahl, S.M., Truitt, M., Olson, P., et al. (2016). Bruton tyrosine kinase–dependent immune cell cross-talk drives pancreas cancer. Cancer Discov. *6*, 270–285.

68. Sautès-Fridman, C., Petitprez, F., Calderaro, J., and Fridman, W.H. (2019). Tertiary lymphoid structures in the era of cancer immunotherapy. Nat. Rev. Cancer *19*, 307–325.

69. Colbeck, E.J., Ager, A., Gallimore, A., and Jones, G.W. (2017). Tertiary lymphoid structures in cancer: drivers of antitumor immunity, immunosuppression, or bystander sentinels in disease? Front. Immunol. *8*, 1830.

70. Zeng, Q., Ng, Y.-H., Singh, T., Jiang, K., Sheriff, K.A., Ippolito, R., Zahalka, S., Li, Q., Randhawa, P., Hoffman, R.A., et al. (2014). B cells mediate chronic allograft rejection independently of antibody production. J. Clin. Invest. *124*, 1052–1056.

71. Gururajan, M., Jacob, J., and Pulendran, B. (2007). Toll-like receptor expression and responsiveness of distinct murine splenic and mucosal B-cell subsets. PLoS One *2*, e863.

72. LeBien, T.W., and Tedder, T.F. (2008). B lymphocytes: how they develop and function. Blood *112*, 1570–1580.

73. Pushalkar, S., Hundeyin, M., Daley, D., Zambirinis, C.P., Kurz, E., Mishra, A., Mohan, N., Aykut, B., Usyk, M., Torres, L.E., et al. (2018). The pancreatic cancer microbiome promotes oncogenesis by induction of innate and adaptive immune suppression. Cancer Discov. *8*, 403–416.

74. Zambirinis, C.P., Pushalkar, S., Saxena, D., and Miller, G. (2014). Pancreatic cancer, inflammation and microbiome. Cancer J. *20*, 195–202.

75. Aykut, B., Pushalkar, S., Chen, R., Li, Q., Abengozar, R., Kim, J.I., Shadaloey, S.A., Wu, D., Preiss, P., Verma, N., et al. (2019). The fungal mycobiome promotes pancreatic oncogenesis via activation of MBL. Nature *574*, 264–267.

76. Riquelme, E., Zhang, Y., Zhang, L., Montiel, M., Zoltan, M., Dong, W., Quesada, P., Sahin, I., Chandra, V., San Lucas, A., et al. (2019). Tumor microbiome diversity and composition influence pancreatic cancer outcomes. Cell *178*, 795–806.e12.

77. Turnis, M.E., Sawant, D.V., Szymczak-Workman, A.L., Andrews, L.P., Delgoffe, G.M., Yano, H., Beres, A.J., Vogel, P., Workman, C.J., and Vignali,

D.A.A. (2016). Interleukin-35 limits anti-tumor immunity. Immunity *44*, 316–329.

78. Rickert, R.C., Roes, J., and Rajewsky, K. (1997). B lymphocyte-specific, Cre-mediated mutagenesis in mice. Nucleic Acids Res. *25*, 1317–1318.

79. Bayne, L.J., Beatty, G.L., Jhala, N., Clark, C.E., Rhim, A.D., Stanger, B.Z., and Vonderheide, R.H. (2012). Tumor-derived granulocyte-macrophage colony-stimulating factor regulates myeloid inflammation and T cell immunity in pancreatic cancer. Cancer Cell *21*, 822–835.

80. Nelson, J.D., Denisenko, O., and Bomsztyk, K. (2006). Protocol for the fast chromatin immunoprecipitation (ChIP) method. Nat. Protoc. *1*, 179–185.

81. Patro, R., Duggal, G., Love, M.I., Irizarry, R.A., and Kingsford, C. (2017). Salmon provides fast and bias-aware quantification of transcript expression. Nat. Methods *14*, 417–419.

STAR★METHODS

KEY RESOURCES TABLE

REAGENT or RESOURCE	SOURCE	IDENTIFIER
Antibodies		
Pax5, 1H9	Biolegend	Cat# 649704; RRID:AB_2562425
Pax5, 1H9	Biolegend	Cat# 649710; RRID:AB_2562573
Pax5, 1H9	Biolegend	Cat# 649707; RRID:AB_2562475
IL-35 (p35), 4D10p35	eBioscience	Cat# 50-7352-82; RRID:AB_2574285
IL-35 (EBi3), 355022	R & D system	Cat# IC18341C; RRID:AB_10890620
IL-35 (EBi3), 355022	R & D system	Cat# IC18341P; RRID:AB_10890620
IL-35 (EBi3), 355022	R & D system	Cat# IC18341A; RRID:AB_10890620
IL-10, JES5-16E3	Biolegend	Cat# 505026; RRID:AB_11150582
IL-10, JES5-16E3	Biolegend	Cat# 505010; RRID:AB_315364
IL-10, JES5-16E3	Biolegend	Cat# 505021; RRID:AB_10900417
IL-10, JES5-16E3	Biolegend	Cat# 505031; RRID:AB_2563146
CD19, 6D5	Biolegend	Cat# 115506; RRID:AB_313641
CD19, 6D5	Biolegend	Cat# 115527; RRID:AB_493734
CD19, 6D5	Biolegend	Cat# 115549; RRID:AB_2563066
CD19, 6D5	Biolegend	Cat# 115545; RRID:AB_2562136
CD19, 6D5	Biolegend	Cat# 115541; RRID:AB_11204087
CD19, 6D5	Biolegend	Cat# 115533; RRID:AB_2259869
CD19, 6D5	Biolegend	Cat# 115519; RRID:AB_313654
pSTAT3, LUVNKLA	ThermoFisher	Cat# 17-9033-42; RRID:AB_2573282
pSTAT3, LUVNKLA	ThermoFisher	Cat# 25-9033-42; RRID:AB_2573536
pSTAT3, LUVNKLA	ThermoFisher	Cat# 12-9033-42; RRID:AB_2572679
CD8, 53-6.7	Biolegend	Cat# 100706; RRID:AB_312745
CD8, 53-6.7	Biolegend	Cat# 100751; RRID:AB_2561389
CD8, 53-6.7	Biolegend	Cat# 100741; RRID:AB_11124344
CD8, 53-6.7	Biolegend	Cat# 100737; RRID:AB_10897101
CD8, 53-6.7	Biolegend	Cat# 100721; RRID:AB_312760
IFN-γ, XMG1.2	Biolegend	Cat# 505810; RRID:AB_315404
IFN-γ, XMG1.2	Biolegend	Cat# 505807; RRID:AB_315401
CD45, 30-F11	Biolegend	Cat# 103137; RRID:AB_2561392
CD45, 30-F11	Biolegend	Cat# 103108; RRID:AB_312973
CD45, 30-F11	Biolegend	Cat# 103125; RRID:AB_493536
CD1d, 1B1	BD Bioscience	Cat# 562712; RRID:AB_2737739
CD1d, 1B1	BD Bioscience	Cat# 553846; RRID:AB_2073521
CD1d, 1B1	BD Bioscience	Cat# 740711; RRID:AB_2740394
IgD, 11-26c.2a	Biolegend	Cat# 405714; RRID:AB_10643423
IgD, 11-26c.2a	Biolegend	Cat# 405729; RRID:AB_2563340
IgD, 11-26c.2a	Biolegend	Cat# 405735; RRID:AB_2563345
CD21, 7E9	Biolegend	Cat# 123407; RRID:AB_940403
CD21, 7E9	Biolegend	Cat# 123415; RRID:AB_1595595
CD21, 7E9	Biolegend	Cat# 123414; RRID:AB_2085158
CD23, B3B4	Biolegend	Cat# 101619; RRID:AB_2563438
CD5, 53-7.3	Biolegend	Cat# 100615; RRID:AB_2260093
CD5, 53-7.3	Biolegend	Cat# 100617; RRID:AB_2562173
CD5, 53-7.3	Biolegend	Cat# 100621; RRID:AB_2562772

(*Continued on next page*)

Continued

REAGENT or RESOURCE	SOURCE	IDENTIFIER
CD27, LG.3A10	Biolegend	Cat# 124209; RRID:AB_1236464
CD4, GK1.5	Biolegend	Cat# 100406; RRID:AB_312691
CD4, GK1.5	Biolegend	Cat# 100427; RRID:AB_493646
CD4, GK1.5	Biolegend	Cat# 100429; RRID:AB_493698
CD25, PC61	Biolegend	Cat# 102035; RRID:AB_11126977
CD25, PC61	Biolegend	Cat# 102012; RRID:AB_312861
Foxp3, MF-14	Biolegend	Cat# 126419; RRID:AB_2565933
Foxp3, MF-14	Biolegend	Cat# 126407; RRID:AB_1089116
CXCR3, CXCR3-173	Biolegend	Cat# 126514; RRID:AB_1186015
CCR5, HM-CCR5	Biolegend	Cat# 107011; RRID:AB_2074528
pSTAT1, Stat1S727-C6	ThermoFisher	Cat# MA5-28057; RRID:AB_2745056
pSTAT1, Stat1S727-C6	ThermoFisher	Cat# MA5-28056; RRID:AB_2745055
pSTAT1, Stat1S727-C6	ThermoFisher	Cat# MA5-37073; RRID:AB_2897008
CD138, 281-2	Biolegend	Cat# 142507; RRID:AB_11204257
CD138, 281-2	Biolegend	Cat# 142521; RRID:AB_2562727
CD138, 281-2	Biolegend	Cat# 142506; RRID:AB_10962911
CXCR4, L276F12	Biolegend	Cat# 146517; RRID:AB_2687244
BCL6, 7D1	Biolegend	Cat# 358514; RRID:AB_2860943
BCL6, 7D1	Biolegend	Cat# 358505; RRID:AB_2562471
BCL6, 7D1	Biolegend	Cat# 358511; RRID:AB_2566195
TNF-α, MP6-XT22	Biolegend	Cat# 506329; RRID:AB_11123912
CD11b, M1/70	Biolegend	Cat# 101237; RRID:AB_11126744
Caspase3, C92-605	BD Bioscience	Cat# 560626; RRID:AB_1727414
CXCR5, L138D7	Biolegend	Cat# 145517; RRID:AB_2562453
CD69, H1.2F3	Biolegend	Cat# 104507; RRID:AB_313110
Ki-67, 16A8	Biolegend	Cat# 652425; RRID:AB_2632693
CD24, ML5	Biolegend	Cat# 311114; RRID:AB_2561284
CD38, HB-7	Biolegend	Cat# 356608; RRID:AB_2561904
CD19, HIB19	Biolegend	Cat# 302225; RRID:AB_493750
CD19, HIB19	Biolegend	Cat# 982406; RRID:AB_2650645
CD19, HIB19	Biolegend	Cat# 302215; RRID:AB_314245
IL-35(p35), SNKY35	ThermoFisher	Cat# 50-7359-42; RRID:AB_11219875
IL-35(EBi3), B032F6	Biolegend	Cat# 360904; RRID:AB_2562880
pSTAT3, 13A3-1	Biolegend	Cat# 651009; RRID:AB_2572087
Pax5, 1H9	Biolegend	Cat# 649709; RRID:AB_2562572
Pax5, D19F8	Cell Signaling Technology	Cat# 8970S; RRID:AB_10950222
pSTAT3, 3E2	Cell Signaling Technology	Cat# 9138S; RRID:AB_331262
pSTAT1, D3B7	Cell Signaling Technology	Cat# 8826S; RRID:AB_2773718
pSTAT3, D3A7	Cell Signaling Technology	Cat# 9145S; RRID:AB_2491009
Pax5, 1H9	ThermoFisher	Cat# 14-9918-95; RRID:AB_2865520
H3K27ac	Abcam	Cat# ab4729; RRID:AB_2118291
HDAC1, D5C6U	Cell Signaling Technology	Cat# 34589S; RRID:AB_2756821
H3K27(me3)	Abcam	Cat# ab6002; RRID:AB_305237
CD19, D4V4B	Cell Signaling Technology	Cat# 90176S; RRID:AB_2800152
CD138	ThermoFisher	Cat# 36-2900; RRID:AB_2533248
H3K27ac	Abcam	Cat# ab4729; RRID:AB_2118291
CD20, MJ1	Leica	Cat# PA0909; RRID:AB_10554604
Ebi3	Sigma	Cat# HPA046635; RRID:AB_2679729

(*Continued on next page*)

Continued

REAGENT or RESOURCE	SOURCE	IDENTIFIER
CD138	R & D System	Cat# MAB2780-SP; RRID:AB_2182840
αCD40, HM40-3	eBioscience	Cat# 16-0402-82; RRID:AB_468945
αCD3	Bio X cell	Cat# BP0001-1; RRID:AB_1107634
αCD28	Bio X cell	Cat# BE0015-1; RRID:AB_1107624
αCD3 (Human)	Bio X cell	Cat# BE0001-2; RRID:AB_1107632
αCD28 (Human)	Bio X cell	Cat# BE0248; RRID:AB_2687729
Human αCD40, 5C3	Biolegend	Cat# 334350; RRID:AB_2810512
Anti-PD1 (*In Vivo*)	Bio X cell	Cat# BP0146; RRID:AB_10949053
IgG2a isotype control	Bio X cell	Cat# BP0089; RRID:AB_1107769
Anti-IL-35 (*In Vivo*), V1.4C4.22	Shenandoah Inc	Cat# MAB-200-IL3522; RRID:AB_11207239
*InVivo*MAb anti-mouse CD20	Bio X Cell	Cat# BE0356; RRID:AB_2894775
IgG2c isotype control	Bio X Cell	Cat# BE0366; RRID:AB_2894738
*InVivo*MAb anti-mouse CD8α	Bio X Cell	Cat# BE0004-1; RRID:AB_1107671
IgG2a isotype control	Bio X Cell	Cat# BE0089; RRID:AB_1107769
Chemicals, peptides, and recombinant proteins		
7-AAD	Biolegend	Cat# 420404
CFSE Cell Division Tracker	Biolegend	Cat# 423801
Rec. IL-10	R & D System	Cat# 417-ML/CF
Rec. IL-35 (Mouse)	Chimerigen Lab	Cat# CHI-MF-11135
Rec. IL-35 (Human)	Chimerigen Lab	Cat# CHI-HF-21035
Rec. IL-12	R & D System	Cat# 419-ML/CF
Rec. IL-23	R & D System	Cat# 1887-ML/CF
Rec. IL-27	R & D System	Cat# 2799-ML/CF
Rec. IL-6	R & D System	Cat# 406-ML/CF
Rec. IL-1β	R & D System	Cat# 401-ML/CF
STA-21 (STAT3 inhibitor)	Santa Cruz Biotechnology	Cat# SC-200757
Fludarabine (STAT1 inhibitor)	Selleckchem	Cat# S1491
79-6 (BCL6 inhibitor)	Selleckchem	Cat# S8250
Bortezomib	EMD Millipore	Cat# 504314
LPS	Sigma	Cat# L2630
Hoechst 33258	ThermoFisher	Cat# H3569
Normal mouse serum	Jackson ImmunoResearch	Cat# 015-000-120
penicillin-streptomycin	Gibco	Cat# 10378016
phorbol 12-myristate 13-acetate (PMA)	Sigma	Cat# P8139
Ionomycin	Sigma	Cat# I3909
Brefeldin A	Biolegend	Cat# 420601
Critical commercial assays		
Thiazolyl Blue Tetrazolium Bromide (MTT)	Millipore-Sigma	Cat# M5655
Duolink™ flowPLA Detection Kit	Millipore-Sigma	Cat# DUO94001
Duolink™ In Situ PLA® Probe Anti-Rabbit PLUS	Millipore-Sigma	Cat# DUO92002
Duolink™ In Situ PLA® Probe Anti-Mouse MINUS	Millipore-Sigma	Cat# DUO92004
Duolink™ In Situ Wash Buffer	Millipore-Sigma	Cat# DUO82047
IgG Mouse ELISA Kit	ThermoFisher	Cat# 8850-40022
IgM Mouse ELISA Kit	ThermoFisher	Cat# 8850-47022
Tissue Extraction Reagent	ThermoFisher	Cat# FNN0071
LDH-Glo cytotoxicity assay kit	Promega	Cat# J2380

(*Continued on next page*)

Continued

REAGENT or RESOURCE	SOURCE	IDENTIFIER
Deposited data		
Bulk RNAseq of naïve murine B cells	This paper	NIH GEO repository accession GSE179797
Plasma cell signature	Newman et al., 2019	Gene Expression Omnibus accession code GSE127472.
Breg signature	Mirlekar et al., 2020	NIH GEO repository accession GSE144504
Experimental models: Cell lines		
KPC 4662	Bayne et al., 2012	N/A
KPC 2173	Bayne et al., 2012	N/A
Experimental models: Organisms/strains		
C57Bl/6J mice	Charles River Labs	stock #027
Il10-/-	Jackson Labs	stock #002251
p35-/-	Jackson Labs	stock #002692
Ebi3-/-	Jackson Labs	stock #008691
μMT	Jackson Labs	stock #002288
KPC	Hingorani et al., 2005	N/A
$Ebi3^{Tom.L/L}$	Turnis et al., 2016	N/A
$CD19^{Cre};Ebi3^{L/L}$	Mirlekar et al, 2020	N/A
Oligonucleotides		
Oligonucleotides	This paper	Table S6
Oligonucleotides can be found in Table S6		
Software and algorithms		
Flowjo software Version 10.2	Tree Star	https://www.flowjo.com/
GraphPad Prism Version 8.0	GraphPad	https://www.graphpad.com/scientificsoftware/prism/s
TFBIND	N/A	https://tfbind.hgc.jp/
TFSEARCH	N/A	http://diyhpl.us/~bryan/irc/protocol-online/protocol-cache/TFSEARCH.html
PROMO-ALGGEN	N/A	http://alggen.lsi.upc.es/cgi-bin/promo_v3/promo/promoinit.cgi?dirDB=TF_8.3
Other		
BD Vacutainer blood collection tubes	BD Biosciences	Cat#367871

RESOURCE AVAILABILITY

Lead contact

Further information and requests for resources and reagents should be directed to and will be fulfilled by the lead contact, Yuliya Pylayeva-Gupta (yuliyap1@email.unc.edu).

Materials availability

Mouse PDAC lines used in this study are available upon request; additionally, the reagents used in this study are available from the lead contact with a completed Materials Transfer Agreement.

Data and code availability

- Bulk murine naïve B cell RNA sequencing data has been submitted to the NIH Gene Expression Omnibus (GEO) repository and is available under accession GSE179797. This manuscript analyzes existing, publicly available data; The accession numbers for the datasets are listed in the key resources table. Microscopy data reported in this paper will be shared by the lead contact upon request.
- Code: This paper does not report original code.
- Any additional information required to reanalyze the data reported in this paper is available from the lead contact upon request.

EXPERIMENTAL MODEL AND SUBJECT DETAILS

Mice

All mouse protocols were reviewed and approved by the Institutional Animal Care and Use Committee of the University of North Carolina at Chapel Hill. Animals were maintained in a specific pathogen-free facility. Six-to-eight-week-old wild-type (WT) C57Bl/6J mice were purchased from The Charles River Laboratories (stock #027). Six- to eight-week-old, *Il10*−/− (stock #002251), *p35*−/− (stock #002692), *Ebi3*−/− (stock #008691) and *μMT* (stock #002288) mouse strains were purchased from The Jackson Laboratory and maintained at UNC. Both male and female mice were used for orthotopic injections of PDAC cells. The $Kras^{LSL\text{-}G12D/+}$;$Trp53^{LSL\text{-}R172H/+}$; $p48^{Cre/+}$ (*KPC*) mice have been described previously.[35] $Ebi3^{Tom.L/L}$ mice were obtained from D. Vignali (University of Pittsburgh, Pittsburgh, PA).[77] $CD19^{Cre}$;$Ebi3^{L/L}$ mice were generated by crossing $CD19^{Cre}$ mice[78] to $Ebi3^{Tom.L/L}$ mice in our colony for two generations to obtain homozygosity at Ebi3 locus. Resulting mice lack expression of Ebi3 in B cells ($B^{Ebi3-/-}$). $CD19^{Cre}$;$Ebi3^{+/-}$ littermates were used as controls. Unless otherwise indicated, experiments were performed using 7–8-week-old mice of indicated genotypes with at least 6-12 mice per group in triplicate.

Cell lines

The murine PDAC cell line *KPC4662* and *KPC2173* were derived from primary pancreatic tumors of C57Bl/6J *KPC* mice by Dr. Vonderheide's laboratory.[79] GFP-labeled *KPC* cells were generated as described previously.[22] Cells were maintained at 37°C and 5% CO2 in complete DMEM (#11995-065, Gibco, 10% FCS and 1% penicillin– streptomycin #15140-122, Gibco) and were confirmed to be Mycoplasma and endotoxin free. Cells were used at <16 passages.

Human samples

The study was carried out in accordance with The University of North Carolina at Chapel Hill School of Medicine guidelines and was approved by institutional review board ethics committees. Informed consent was obtained from the patients and healthy donors before blood donation. The study (study #9001, IRB #90-0573) was conducted in accordance with ethical standards such as the Declaration of Helsinki. Samples analyzed included splenic immune cells isolated from PDAC patients, where human resected spleen samples were collected from 25 patients with pancreatic ductal adenocarcinoma, and tumor microarray containing normal adjacent and PDAC tumor samples. All samples were received as de-identified, therefore, the information on the age and/or gender of the donors is not available.

Primary lymphocyte cells

Primary mouse or human lymphocytes, including naïve B cells, regulatory B cells (Breg), conventional B cells (Bcon) and T cells were isolated and maintained in complete RPMI media containing 10% FCS with 1X penicillin–streptomycin (#15140-122, Gibco) antibiotics for 24-72hr. Details of specific culture conditions is described below.

In vitro culture of primary B and T cells

Sorted naïve B, Breg and Bcon cells were activated with 1 μg/ml αCD40, 2 μg/ml LPS and/or rIL-35 (50 ng/ml), rIL-12 (20 ng/ml), rIL-10 (20 ng/ml), rIL-23 (20 ng/ml) and rIL-27 (20 ng/ml) as indicated. Naïve B cells were cultured for 72 hrs, while Breg and Bcon cells were cultured for 48 hrs at 37°C and 5% CO2. Sorted T cells were stimulated with 1 μg/ml αCD3 and 2 μg/ml αCD28 for 48 hrs prior to PMA/Ionomycin stimulation. For *in vitro* $CD8^+$ T-cell culture, splenic $CD8^+$ T cells specific for the OVA257-264 (InvivoGen) antigen were sorted (>98% purity) from WT mice immunized with OVA257-264 for 1 week (10 μg/mouse). T cells were cultured with plate bound αCD3 (1 μg/mL, Bio X Cell) and soluble αCD28 (2 μg/mL, BioXCell), for 48 hrs.

METHOD DETAILS

Bone marrow mouse chimera generation

B^{WT} and $B^{p35\text{-}/\text{-}}$ mice were obtained by a mixed bone marrow chimera method, as described in reference no 28 [28]. Briefly, B^{WT} and $B^{p35\text{-}/\text{-}}$ mice were obtained by a mixed bone marrow chimera method using lethally irradiated (1,000 cGy radiation delivered from cesium source) using C57BL/6J mice as recipients. Recipients were reconstituted with a mixture of bone marrow cells from B cell–deficient *μMT* mice (The Jackson Laboratory, #002288) or WT C57BL/6J mice (80%), respectively, and $p35^{-/-}$ mice (20%; The Jackson Laboratory, #002692). A total of 10×10^6 bone marrow cells was injected intravenously into the irradiated WT recipients. The chimeric animals were used after eight weeks and specific deletion of *p35* gene in B cells was confirmed by PCR.

Mouse tumor cell injection studies

For intrapancreatic injection of cancer cells, mice were anesthetized using a ketamine (100 mg/kg)/xylazine (10 mg/kg; Med-Vet International) cocktail. The depth of anesthesia was confirmed by verifying an absence of response to toe pinch. An incision in the left flank was made, and 75,000 KPC cells in ice-cold PBS mixed at 1:1 dilution with Matrigel (#354234, Corning) in a volume of 50 μL were injected using a 28-gauge needle into the tail of the pancreas. The wound was closed in two layers, and the animals were given the pain reliever buprenorphine (0.1 mg/kg; Med-Vet International) once subcutaneously after orthotopic surgery. To analyze the

functional effects of plasma cells, we treated mice intravenously with 0.75 mg/kg body weight bortezomib (Millipore-sigma) twice weekly and control mice with equivalent volume of solvent PBS for 3 weeks. After 3 weeks, mice were sacrificed for tumor analysis.

Mouse tumor treatment studies

For therapeutic treatment with immune checkpoint blockade, anti–PD-1 (RMP1-14, Bio X Cell) or their respective IgG isotype controls were injected at 200 μg/injection on days 7, 9, and 11, once an orthotopic tumor reached 4 to 5 mm (day 7). Three doses of antibody were given in total, on days 7, 9, and 11 after injection of *KPC* cells and mice were sacrificed after 3 weeks for tumor analysis.

Lymphocyte isolation

Single-cell suspensions were prepared from tumors and spleens isolated from orthotopic and/or adoptive transfer models. Spleens were mechanically disrupted using the plunger end of a 5 mL syringe and re-suspended in 1% FBS/PBS. Spleen samples were processed following RBC lysis (eBioscience; 00-4333-57). For isolation of tumor-infiltrating lymphocytes, tumor tissue was minced into 1 to 2 mm pieces and digested with collagenase IV (1.25 mg/mL; #LS004188, Worthington), 0.1% soybean trypsin inhibitor (#T9128, Sigma), hyaluronidase (1 mg/mL; #LS002592, Worthington), and DNase I (100 μg/mL; #LS002007, Worthington) in complete DMEM for 30 minutes at 37°C. Cell suspensions were passed through a 70-μm cell strainer (Falcon) and resuspended in RPMI media (Gibco). Lymphocytes were isolated from processed tumor tissues by OptiPrep (Sigma) density gradient centrifugation. MACS isolation of total $CD45^+$ leukocytes (MACS Miltenyi Biotec #130-052-301) was performed on the leukocyte-enriched fraction according to Miltenyi Biotec protocol, and the purity was >90%. Cells were stained with fluorophore-labeled antibodies for 30 minutes on ice in FACS buffer (PBS with 3% FCS and 0.05% sodium azide). After staining, cells were washed twice with FACS buffer and resuspended in sorting buffer (PBS with 1% FCS and 0.05% sodium azide). Cell sorting using a BD FACS ARIA III sorter was performed to isolate $CD19^+IgD^{hi}CD1d^-CD27^-$ naïve B cells, $CD19^+CD21^{hi}CD5^+CD1d^{hi}$ regulatory B cells (Breg), $CD19^+CD21^{lo}CD5^-CD1d^-$ conventional B cells (Bcon), $CD4^+$ and $CD8^+$ T cells. Cells were collected in complete RPMI media containing 10% FCS with 1X penicillin–streptomycin (#15140-122, Gibco) antibiotics. More than 97% purity was achieved.

Breg and Bcon cell isolation from human spleen

Spleen samples were processed as described above by mechanically disrupting followed by RBC lysis. The isolated splenocytes were then stained with anti-human CD19 (HIB19; BioLegend), CD24 (ML5; BioLegend), and CD38 (HB-7; BioLegend) in FACS buffer for 20 minutes on ice. $CD19^+CD24^{hi}CD38^{hi}$ Bregs and $CD19^+CD24^{lo}CD38^{lo}$ Bcon cells were sorted using a BD FACS ARIAIII, and cells were collected in complete RPMI media. More than 97% cell purity was achieved.

MTT assay

The viability of *KPC 4662* cells with 10, 200, 500 and 1000 nMol of bortezomib were assessed with MTT (Sigma #M5655) as per manufacturer instructions. Briefly, the 10μL from 5 mg/mL MTT stock was added in each well of a 96 well plate and incubated at 37°C for 3 hours. After incubation, 150μL of DMSO were added in each well and plate was kept on orbital shaker for 15 min and was read within 1 hr at 590nm.

B cell: T cell co-culture

Mouse splenic Bregs ($CD19^+CD21^{hi}CD5^+CD1D^{hi}$) were sorted by flow cytometry from spleens of WT, *KPC*, and tumor-bearing *Il10*−/−, *p35*−/− and *EBi3*−/− mice (>97% purity), as described above. A total of 100,000 Bregs or Bcon cells and 100,000 $CD4^+$ or $CD8^+$ T cells (1:1 ratio) were co-cultured in the 96-well Transwell plates, with B cells occupying the top chamber and $CD4^+$ or $CD8^+$ T cells the bottom chamber (Corning; 3381) for 48 hrs. B cells were activated by αCD40 (1 μg/mL, eBioscience) and LPS (2 μg/mL, Sigma) for 48 h, and T cells were activated by plate bound αCD3 (1 μg/mL) and soluble αCD28 (2 μg/mL). Cytokine secretion of T cells was evaluated by flow cytometry, as described below. For co-culture of B cells with T cells from PDAC patients, splenic $CD19^+CD24^{hi}CD38^{hi}$ Bregs and $CD19^+CD24^{lo}CD38^{lo}$ Bcon cells were sorted by flow cytometry (>97% purity), as described above. The Breg or Bcon cells were co-cultured with $CD4^+$ or $CD8^+$ T cells in 1:1 ratio and activated as described above and the expression of effector cytokines from T cells was evaluated by qPCR analysis of gene expression, as described below.

In vitro treatment and adoptive transfer of B cells

Naïve B cells ($CD19^+IgD^{hi}CD1d^-CD27^-$) were isolated from spleens of *KPC* mice by BD FACS-ARIA III flow cytometry sorting (purity >98%). Sorted naïve B cells were treated with αCD40 (1 μg/mL), LPS (2 μg/mL), rIL-35 (50 ng/mL) with or without BCL6 and STAT inhibitors; STA-21 (20 μmol/L) for STAT3 (Santa Cruz Biotechnology), Fludarabine (50 μmol/L) for STAT1 (Selleckchem) and 79-6 (100 μmol/L) for BCL6 for 72 hrs. The viability and proliferation of naïve B cells and purified Breg cells treated with STAT1 and STAT3 inhibitors were assessed with MTT (Sigma #M5655) as per manufacturer instructions. After 72 hrs, 10 x 10^6 control or BCL6 and STAT inhibited cells were adoptively transferred via tail vein injection into B cell deficient *μMT* mice. One day after adoptive transfer, 75,000 *KPC4662* cells were orthotopically transplanted into the pancreas of *μMT* mice. Recipient mice were sacrificed 21 days post-tumor cell injections, tumor size and weight were measured, and spleens and tumors were collected for further processing and analysis.

Intracellular cytokine and transcription factor staining

For *ex vivo* stimulation, sorted cells from tumors or spleens of orthotopic and/or adoptive transfer models (except for B cells, which were cultured in LPS and αCD40 prior to this step) were incubated with PMA (50 ng/mL; Sigma, #P8139) and ionomycin (200 ng/mL; Sigma, #I0634) in the presence of Golgistop Brefeldin A (1X, BioLegend) in complete RPMI medium for 5 hrs at 37°C. Cells were washed and blocked with αCD16/CD32 (Fc Block, BD Biosciences, 0.1 mg/100,000 cells) for 5 minutes on ice. Viability was assessed using the Live/Dead 7AAD (BioLegend; 420404) stain solution or Live/Dead Aqua cell stain kit (Life Technologies). Cells were then washed and stained with labeled antibodies against surface markers on ice for 30 minutes in FACS buffer (PBS with 3% FCS and 0.05% sodium azide). After surface staining, cells were washed, fixed, and permeabilized using cytofix/cytoperm buffer (BD, 554714) for 15 minutes at 4°C in the dark. Intracellular staining was performed using fluorophore-conjugated cytokine antibodies for 1 hr at 4°C in the dark. After intracellular staining, cells were washed and resuspended in FACS buffer for acquisition by flow cytometry. Intracellular staining for Foxp3 was performed using a Foxp3 staining kit (eBioscience, catalog no. 00-5523). Intracellular staining for transcription factors in B cells was performed by using True-Nuclear Transcription Factor Buffer Set (Biolegend; 424401). Briefly, after cell surface staining described above, cells were fixed using True-Nuclear 1X Fix Concentrate at room temperature (RT) in dark for 45 minutes. Cells were washed two times with the True-Nuclear 1X Perm Buffer and a secondary fluorochrome-conjugated antibody diluted in True-Nuclear 1X Perm Buffer was added. Cells were incubated at RT in dark for 1 hr. After incubation, cells were washed 2 times with the True-Nuclear 1X Perm Buffer and resuspended in FACS buffer for acquisition by flow cytometry. For staining of phosphoproteins, cells were fixed with fixation buffer (BioLegend; 420801) at room temperature for 10 minutes and permeabilized with True-Phos perm buffer (BioLegend; 425401) at −20°C overnight. Cells were then washed twice and resuspended in cell staining buffer (BioLegend; 420201). Fluorophore-conjugated phosphoprotein cocktail antibodies or isotype controls were added and incubated for 60 minutes at 4°C. After incubation, cells were washed, resuspended in FACS buffer, and samples were acquired on LSR II and LSRII Fortessa (BD Biosciences) and analyzed with FlowJo version 10.2 (TreeStar, Inc.). The human splenic B cells were processed as described above, but the blocking step was done with human BD Fc Block (BD Biosciences, 564219, 0.1 mg/100,000 cells) for 5 minutes on ice. All antibodies and reagents are listed in the key resources table.

ChIP and ChIP-re-ChIP

ChIP assays were performed as described previously.[80] Briefly, sorted naïve B cells or Breg cells from tumor-bearing or healthy mice were stimulated with αCD40 (1 μg/ml), LPS (2 μg/ml) and rIL-35 (50 ng/mL) for 72hr and 48hr respectively. After activation and cytokine treatment cells were harvested and cross-linked with 37% (W/V) formaldehyde at final concentration of 1.42% for 15 min at RT. Formaldehyde quenching was done with 125 mM glycine for 5 min at RT. Cell lysis was performed using IP buffer (150 mM NaCl, 50 mM Tris-HCl pH 7.5, 5 mM EDTA, 0.5% V/V NP-40 and 1% V/V Triton X-100). Chromatin was sheared into fragment sizes 500-1000 base pairs in length with four rounds of 15 sec sonication with a 2 min rest between each round using a Diagenode Bioruptor. Sheared chromatin was then subjected to immunoprecipitation with different transcription factor and histone modifier antibodies (key resources table) with isotype matched control antibodies, followed by overnight incubation with rotation. DNA-protein complexes were immune-precipitated with protein A-agarose beads, washed with IP buffer to remove ethanol. Immunoprecipitation with protein A-agarose beads was performed at 4°C for 1 hr on a rotating platform. The beads were then washed with IP buffer without inhibitors and subjected for DNA isolation. The DNA isolation was performed using 10% (W/V) chelex-100 slurry followed by precipitation of DNA with 70% ethanol. For ChIP-re-ChIP, the DNA-protein complexes were eluted with 0.1 M dithiothreitol followed by a second round of immunoprecipitation with a specific transcription factor antibody, washes with IP buffer and elution with Sodium bicarbonate. DNA was purified using 10% (W/V) chelex-100 slurry followed by precipitation with 70% ethanol. Purified DNA was used to perform real-time PCR with SYBR green master-mix in 10 μL reaction volume (2.5 μL DNA template, 0.3 μL of 10 μM primer pair, 5 μL master-mix and 2.2 μL PCR grade water). Relative occupancy of the immune-precipitated factor at the locus is estimated by using $2^{-}(Ct^{control} - Ct^{sample})$ equation. Relative enrichment of upstream of transcriptional start site (TSS) is shown and results are scaled to ChIP with control isotype antibody and input. The primers used to perform PCR are listed in key resources table.

QPCR analysis for gene expression

RNA was extracted from treated cells using the RNeasy Micro Kit (Qiagen). cDNA was generated using High-Capacity cDNA-RT Kit (Invitrogen). QPCR analysis (with 100 ng of DNA template) was performed using the SSO advanced universal SYBR green super-mix reagent (Bio-Rad) and Applied Bio-System platform. Results were normalized to the expression of *β-actin*, and each sample was run in triplicate. Gene expression was determined by the ΔΔCt method ($2^{-\Delta\Delta Ct}$). Primer sequences are listed in key resources table. *β-actin* was used to normalize the data by the ΔCt method.

Proximity ligation assay

Protein interaction between STAT3 and Pax5 was detected by Duolink proximity ligation assay (PLA; Sigma-Aldrich). Splenic naïve B cells from *KPC* mice and intratumoral Breg cells from control, $B^{EBi3-/-}$ and $B^{p35-/-}$ mice were sorted using BD FACS-ARIAIII sorter. Naïve B cells were treated with αCD40/LPS and recombinant cytokines for 72 hrs as indicated above. Breg cells were treated with αCD40/LPS for 48 hrs. After incubation, cells were processed for Duolink proximity ligation assay. Anti-Pax5 (Rabbit) and Anti-pSTAT3 (Mouse) antibodies were conjugated with Duolink *In Situ* PLA Probe anti-Rabbit PLUS and Duolink *In Situ* PLA Probe anti-Mouse MINUS (Sigma-Aldrich) respectively. Duolink flow cytometry protocol was followed with few modifications. Briefly,

treated naïve B and Breg cells were fixed and permeabilized using BD cytofix/cytoperm buffer (BD Bioscience) followed by blocking with anti-CD16/CD32 (Fc Block, BD Biosciences, 0.1 mg/100,000 cells) for 5 minutes on ice. Samples were incubated with primary anti-rabbit Pax5 PLA-PLUS and anti-mouse pSTAT3 PLA-MINUS antibodies for 1hr at 37°C. Ligation, amplification and detection were performed using Duolink flow PLA Detection Kit - Red (Sigma-Aldrich) kit, following manufacturer's instructions. Duolink technical negative control contained only PLA probes but neither Pax5 PLUS nor pSTAT3 MINUS antibodies. The samples were analyzed by LSRII-Fortessa (BD Bioscience) and analyzed by FlowJo version 10.2 (TreeStar, Inc.).

RNAseq library preparation and analysis

Naïve B cells ($CD19^{+}IgD^{hi}CD1d^{-}CD27^{-}$) were isolated from spleens of non-tumor bearing and tumor bearing WT and $B^{EBi3-/-}$ mice (two biological replicates per condition) by BD FACS-ARIA III flow cytometry sorting (purity >98%). Sorted naïve B cells were subjected for RNA isolation using the RNeasy Micro Kit (Qiagen). RNAseq Libraries were prepared using the TruSeq Stranded mRNA Library Prep (Illumina, 20020594). In this process, mRNA was isolated using polyA-selection by incubation with poly-T oligo attached magnetic beads. mRNA was then fragmented under elevated temperature with divalent cations. First strand cDNA was generated using reverse transcriptase and random primers with the addition of actinomycin D. Second strand cDNA was generated using DNA Polymerase I with RNase H, and the reaction quenched with the incorporation of dUTP. The 3′ ends were adenylated and dual index adapters ligated using the kit's DNA Ligase enzyme. The final cDNA strands with adapters were amplified to produce the final libraries, which were pooled and diluted to 1.65pM before being sequenced on a NextSeq500 using the NextSeq 500/550 Mid Output Kit v2.5 (150 Cycles) (Illumina, 20024904). Using the bcl2fastq2 Conversion software 2.20.0 we converted BCL files to FASTQ files and then collapsed the lanes into one file. Total expected read counts were quantified using Salmon 0.9.1(1) using arguments "–gcBias –seqBias". The UCSC mouse reference genome mm10 used to quantify reads.[81] Count data was loaded into R v3.6.3 with tximport v1.12.3, and differential expression analysis was performed using the DESeq2 v1.24.0. Heat maps generated with pheatmap v1.0.12 using the variance stabilized transform (VST). PCA plots generated using both VST data and FactoExtra 1.0.7 library. Gene ontogeny analysis was performed using IPA.

Luciferase reporter assay

Transient luciferase reporter transfection assay was performed in HEK 293T cell line using *EBi3*, *p35* and *Cd1d* promoter luciferase reporter constructs. The STAT3 and Pax5 binding sites on *EBi3*, *p35* and *Cd1d* promoter were identified by ChIP. We selected regions −1600 for *EBi3*, -2200 for *p35* and -500 for *Cd1d* promoters. Mutations in the cloned promoter regions were designed by deleting STAT3-Pax5 binding consensus sequences (Figures 5I–5K). The WT and mutant sequences were cloned into construct containing luciferase reporter and all the WT and mutant vectors were generated by VectorBuilder Inc (Chicago, IL). The WT and mutant constructs were then transfected using Lipofectamine (Sigma-Aldrich) into HEK293T cells. After transfection, the cells were left untreated or treated with IL-6 (20 ng/mL) for 24 hrs. After 24 hrs, cells were processed for luciferase assay using Dual-Luciferase Reporter Assay system (Promega) as per manufacturer instructions and luminescence were measured in single photon counting (SPC) mode on the SpectraMax i3x. Full sequences of *EBi3*, *p35* and *Cd1d* gene promoter wild-type and mutant constructs will be attached as Supplementary files following acceptance of the manuscript.

Enzyme-linked immunosorbent assay (ELISA)

Tumor homogenates were prepared by homogenizing tumor tissue with Tissue Extraction Reagent I (ThermoFisher; FNN0071, 50 mM Tris, pH 7.4, 250 mM NaCl, 5 mM EDTA, 2 mM Na3VO4, 1 mM NaF, 20 mM Na4P2O7, 0.02% NaN3, detergent). The Phosphatase inhibitor cocktail, Protease inhibitor cocktail and PMSF were added just prior to use. Samples were incubated at 4°C for 1 hr on the orbital shaker and supernatants were collected by centrifuging the tubes at 9000 rpm for 10 min at 4°C. All samples were stored at −80°C. The concentration of IgG was measured using mouse IgG ELISA kit (ThermoFisher; 88-50400-22) and concentration of IgM was measured using mouse IgM ELISA kit (ThermoFisher; 88-50470-22) according to manufacturer's instructions.

Antibody-dependent cellular cytotoxicity (ADCC)

Effector cells were peripheral blood mononuclear cells (PBMC) obtained from C57B6/J mice on the same day of the experiment using BD vacutainer tube with sodium heparin (BD Biosciences). For the cytotoxicity assay, effector cells were cultured with target cells (non-cancerous pancreatic cells or tumor cells) at 20:1 (E:T) ratio with and without serum samples from tumor bearing WT, $B^{EBi3-/-}$ and $B^{p35-/-}$ mice. After incubation for 6 hrs at 37°C a cell cytotoxicity assays (LDH-Glo Cytotoxicity Assay, J2380 Promega) were performed according to manufacturer's instructions.

Depletion of $CD8^{+}$ T cells, and αIL-35 treatment *in vivo*

For $CD8^{+}$ T cell depletion studies, 200 μg of anti-CD8 (Bio X Cell, BP0004-1, clone 53-6.7) or an IgG isotype control (Bio X Cell), were administered intra-peritoneally daily starting 3 days prior to tumor cell injection and twice a week after tumor cell injection. *In vivo* IL-35 blockade was described previously.[28] Mice were sacrificed 21 days after tumor implantation, tumor size, and weight were measured, and spleen and tumor samples were collected for further processing. Depletion of cells was confirmed by flow cytometry at the end of the experiment.

Immunohistochemistry

Mouse tumor tissues were fixed in 10% buffered formalin (Fisher Scientific) for 48hr. Tissues were then washed in 70% ethanol and embedded in paraffin at the Histology Core. Six-micrometer sections were treated with xylenes and rehydrated. Endogenous peroxidase activity was quenched using a solution of 1% hydrogen peroxide (stock of 30% hydrogen peroxide, Sigma) in methanol at room temperature for 10 minutes. Antigen retrieval was done in a microwave oven using 10 mmol/L sodium citrate with 0.05% Tween-20 solution (pH 6.1) for 15 minutes. Blocking was performed for 1 hour at room temperature in a solution of 10% goat serum, 10 mmol/L Tris–HCl, 0.1 mol/L magnesium chloride, 1% BSA, and 0.5% Tween-20. Sections were incubated with primary rat anti-CD19 (Cell Signaling Technology #90176T clone D4V4B) or anti-CD138 (Thermo Fisher #36-2900) diluted in 2% BSA/PBS (CD19 1:400 and CD138 1:200) overnight at $4C^0$. Secondary biotinylated goat anti-rabbit (1:400 final concentration of 3.75 mg/mL) and incubated for 1 hour at room temperature. Tertiary ABC solution was prepared according to the manufacturer's instructions (Vectastain ABC kit, Vector Laboratories) and incubated with slides for 45 minutes at room temperature. Sections were developed using a 3,30-diaminobenzidine tetrahydrochloride kit (DAB peroxidase substrate kit, Vector Laboratories). Slides were then counterstained with Harris hematoxylin (Sigma), dehydrated, and mounted with DPX mounting media (Sigma). Images were acquired using Nikon Eclipse Ni-U microscope with NIS-Elements software (Nikon). $CD138^+$ plasma cells were counted per 20x FOV, counting 3-6 FOV per tumor sample.

Immunofluorescence on human tissues

Slides containing fluorescently labeled tissue sections (56 tumor samples and 23 normal adjacent) were scanned in the Aperio ScanScope FL (Leica Biosystems) using the 20x objective and images were archived in TPL's eSlide Manger database (Leica Biosystems). For analysis, expression of CD20, EBi3, CD138 and pan-Cytokeratin was assessed using ImageJ (Fiji). Analysis data included the percentage of CD20, EBi3 co-expressing (Breg) cells and CK^-CD138^+ expressing plasma cells and the correlation between Breg cells and plasma cells for each antibody marker.

Human immunoregulatory B cell signature

B cell signature derived in Mirlekar et al., 2020[28] was used. Briefly, RNA-seq library was prepared from human PBMC conventional and immunoregulatory B-cell populations from healthy volunteers and treatment-naïve PDAC patients. Sequencing was performed on the Illumina HiSeq4000 platform using 150 bp paired-end chemistry and targeting 9×10^7 reads per sample. FASTQ files were aligned to the human reference genome using STAR v2.4.2. The BAM output files were then quantified using Salmon v0.8.2. FastQC v0.11.7 and MultiQC v1.5 was used to generate quality assurance reports. Statistical analyses were executed in R v3.3.3. Differential gene expression analysis was conducted on the resulting expression matrices using the DESeq2 R package. Genes that were found to be differentially upregulated in tumor-associated Breg subtypes compared with Bcon subtypes, with a Benjamin–Hochberg corrected p value of less than 0.1, were identified. Breg signature was calculated by taking the geometric mean of the expression values of the identified genes.

QUANTIFICATION AND STATISTICAL ANALYSIS

At least 9 to 21 mice were used in each group, with a minimum of 6 mice in each group per experiment, and the experiments were repeated a 2-3 times to validate reproducibility. Before analysis, data were examined for quality. Group means were compared using Student t-test. Significance in variations between two groups was determined by unpaired Student t-test (two-tailed), experiments with more than two groups used one-way ANOVA comparison; when two groups were tested for more than one condition two-way ANOVA was used. Statistical analysis was performed using GraphPad Prism software. Data are presented as mean± SEM. $p < 0.05$ was considered statistically significant. CIBERSORTx was used to determine the percent of plasma cells in each PAAD TCGA sample (plasma cell signature).[33] This value was compared to the Breg signature score using Spearman's rank correlation coefficient. Cox proportional hazard model was used to determine the hazard ratio for the plasma cell signature. A T-test was performed to compare the gene expression between conventional B cells and Breg in PAAD samples for select genes. TCGA expression matrices were accessed at http://firebrowse.org.